

Aerosol microphysics simulations of the Mt. Pinatubo eruption with the UKCA composition-climate model

S. S. Dhomse¹, K. M. Emmerson², G. W. Mann^{1,3}, N. Bellouin⁴, K. S. Carslaw¹, M. P. Chipperfield¹, R. Hommel^{5,*}, N. L. Abraham^{3,5}, P. Telford^{3,5}, P. Braesicke^{3,5,}, M. Dalvi^{3,6}, C. E. Johnson⁶, F. O'Connor⁶, O. Morgenstern⁷, J. A. Pyle^{3,5}, T. Deshler⁸, J. M. Zawodny⁹, and L. W. Thomason⁹**

¹School of Earth and Environment, University of Leeds LS2 9JT, UK

²CSIRO Marine and Atmospheric Research, Aspendale, Victoria 3195, Australia

³National Centre for Atmospheric Science (NCAS-Climate), UK

⁴Department of Meteorology, University of Reading, Reading, UK

⁵Department of Chemistry, University of Cambridge, Cambridge, UK

⁶Met Office, Exeter, UK

⁷National Institute of Water and Atmospheric Research (NIWA), Lauder, New Zealand

⁸University of Wyoming, Wyoming, USA

⁹NASA Langley Research Center, Hampton, Virginia, USA

* now at: IUP, University of Bremen, Bremen, Germany

** now at: IMK-ASF Karlsruhe Institute of Technology, Karlsruhe, Germany

Correspondence to: S. S. Dhomse (s.s.dhomse@leeds.ac.uk)

Abstract

We use a stratosphere-troposphere composition-climate model with interactive sulphur chemistry and aerosol microphysics, to investigate the effect of the 1991 Mount Pinatubo eruption on stratospheric aerosol properties. Satellite measurements indicate that shortly after the eruption between 14 and 23 Tg of SO₂ (7 to 11.5 Tg of sulphur) was present in the tropical stratosphere. Best estimates of the peak global stratospheric aerosol burden are in the range 19 to 26 Tg, or 3.7 to 6.7 Tg of sulphur assuming a composition of between 59 and 77% H₂SO₄. In light of this large uncertainty range, we performed two main simulations with 10 and 20 Tg of SO₂ injected into the tropical lower stratosphere. Simulated stratospheric aerosol properties through the 1991 to 1995 period are compared against a range of available satellite and in-situ measurements. Aerosol optical depth (AOD) and effective radius from both simulations show good qualitative agreement with the observations, with the timing of peak AOD and decay timescale matching well with the observations in the tropics and mid-latitudes. However, injecting 20 Tg gives a factor two too high stratospheric aerosol mass burden compared to the satellite data, with consequent strong high biases in simulated AOD and surface area density, with the 10 Tg injection in much better agreement. Our model cannot explain the large fraction of observed sulphur injection that was removed within first few months after the eruption. This indicate that there must be an additional alternative loss pathway for the SO₂, possibly involving ash or ice in the volcanic cloud that is not included in our model.

We also critically evaluate the simulated evolution of the particle size distribution, comparing in detail to balloon-borne optical particle counter (OPC) measurements from Laramie, Wyoming, USA (41° N). Overall, the model captures remarkably well the complex variations in particle concentration profiles across the different OPC size channels. However, for the 19 to 27 km injection height-range used here, both runs have a modest high bias in the lowermost stratosphere for the finest particles (radii less than 250nm), and the decay timescale is longer in the model for these particles, with

a much later return to background conditions. Also, whereas the 10 Tg run compared best to the satellite measurements, a significant low bias in the coarser size channels is apparent in the volcanically perturbed lower stratosphere. Nevertheless, our results suggest that, with appropriate calibration, aerosol microphysics models are capable of capturing the observed variation in particle size distribution in the stratosphere across both volcanically perturbed and quiescent conditions. Furthermore, additional sensitivity simulations suggest that predictions with the models are robust to uncertainties in sub-grid particle formation and nucleation rates in the stratosphere.

1 Introduction

Volcanic eruptions can have significant impacts on atmospheric composition and climate (e.g. McCormick et al., 1995; Robock, 2000). Powerful explosive eruptions can inject large amounts of SO_2 , ash, water vapour and various other chemical species directly into the stratosphere. Volcanic SO_2 injected into the stratosphere is chemically converted to sulphuric acid vapour over a timescale of days to months, causing substantial new particle formation and aerosol growth by condensation. Volcanic enhancements of the stratospheric aerosol can be long lasting in the case of tropical eruptions with optically-active particle concentrations substantially enhanced for several years (Deshler et al., 2003). The perturbed stratospheric aerosol alters the Earth's radiative balance with increased albedo via enhanced back-scattering of solar radiation, cooling the surface and increased absorption of terrestrial long-wave radiation, warming the stratosphere (Labitzke and McCormick, 1992). The relative magnitude of these short wave and long wave radiative effects are strongly influenced by its particle size distribution (Lacis et al., 1992; Hansen et al., 1992).

The long-wave radiative heating induced by the thicker aerosol layer also modifies the stratospheric circulation (e.g. Young et al., 1994), leading to indirect radiative effects via dynamical changes in ozone and meridional transport, with important implications for surface climate (Robock and Mao, 1992; Graf et al., 1993). Volcanically increased

aerosol surface area density (SAD) can also accelerate heterogeneous chemistry perturbing stratospheric NO_y species, halogens and ozone (e.g. Solomon et al., 1996). Quantifying the net impact from these direct and indirect radiative effects is very important to better understand volcanic influences within the historical climate records.

5 There is an increasing recognition that having a good representation of stratospheric processes is important for climate projections (e.g. Scaife et al., 2012). However, whereas most coupled atmosphere-ocean climate models (e.g. Jones et al., 2011) that carried out historical integrations for CMIP5 (Taylor et al., 2012) included a prognostic treatment of tropospheric aerosol, stratospheric aerosol are treated separately.
10 Some models impose volcanic forcings and heating rates (e.g. Stenchikov et al., 1998) or base these on prescribed time-varying aerosol optical depth climatologies such as Sato et al. (1993). None of the CMIP5 climate models are able to capture the complex dynamical changes associated with large tropical eruptions (Driscoll et al., 2012). There is now an established group of composition-climate models (CCMs) which simulate stratospheric chemistry with interactive ozone radiative effects (e.g. SPARC, 2010),
15 but few include prognostic treatment of stratospheric aerosol. Even relatively modest changes in stratospheric aerosol can exert a significant radiative forcing (e.g. Solomon et al., 2011) and expected future changes in stratospheric circulation further motivate the need for interactive stratospheric aerosol in climate models.


20 We use the stratosphere-troposphere composition-climate model UMUKCA (Unified Model – UK Chemistry and Aerosol) to simulate stratospheric aerosol interactively. The model includes the GLOMAP-mode aerosol scheme and calculates aerosol optical properties online and consistently with the 3-D evolution of the particle size distribution, as driven by the underlying microphysical processes. We use the 1991 Mount
25 Pinatubo eruption as a test case to examine simulated aerosol properties comparing to a range of satellite and in-situ observations covering the background, volcanic perturbation and decay periods. Pinatubo erupted in the Philippines (15.1° N, 120.4° E) on 15 June 1991 and was the largest tropical eruption since Krakatoa 1883. Column SO₂ mass loadings derived from ultra-violet radiation measurements from the Total Ozone

Monitoring Spectrometer (TOMS) instrument Bluth et al. (1992) estimated that the eruption injected approximately 20 Tg into the tropical stratosphere. Guo et al. (2004a) re-evaluated the post-Pinatubo TOMS data, and also analysed measurements from the Television Infra-red Observation Satellite Vertical Sounder (TOVS), finding total SO₂ released to be in the range 14 to 23 Tg (7 to 11.5 Tg of sulphur).

Assuming a 50 % conversion of SO₂ to sulphuric acid by July and using an assumed size distribution and composition to convert the Stratospheric Aerosol and Gas Experiment II (SAGE-II) satellite measurements of aerosol extinction, McCormick and Veiga (1992) estimated that the total global aerosol loading was increased by 20 to 30 Tg. Baran and Foot (1994) used infrared satellite measurements from the High resolution Infrared Radiation Sounder (HIRS) instrument to derive a timeseries of the global stratospheric aerosol mass loading, finding a peak of 21 Tg in September 1991 with values in excess of 15 Tg persisting until November 1992 and much earlier and steeper decay in the tropics than Northern Hemispheric mid-latitudes. Lambert et al. (1993) found a peak aerosol loading of 19 to 26 Tg from the Improved Stratospheric and Mesospheric Sounder (ISAMS) measurements, which assuming the aerosol composition ranges from 59% to 77% sulphuric acid (Grainger et al., 1993), translates into an aerosol sulphur burden uncertainty range of 3.7 to 6.7 Tg of sulphur. Taken together these findings suggest a large proportion of the sulphur was removed from the stratosphere within the first few months after the eruption, with potential loss pathways involving sedimentation, cross-tropopause transport out of the stratosphere (Deshler, 2008) or enhanced removal via interactions with ash or ice in the Pinatubo cloud (Guo et al., 2004b). Monthly balloon soundings of total and size-resolved particle concentrations carried out at Laramie, Wyoming (e.g. Deshler, 1994) showed that although substantially enhanced particle concentrations were detected in the lower-most stratosphere by mid-July, the main part of the volcanic plume was only transported to Northern Hemisphere (NH) mid-latitudes several months later.

There have been many previous global modelling studies to simulate the evolution of the stratospheric aerosol following the Pinatubo eruption. However most have used

aerosol schemes that simulate only the evolution of aerosol mass, prescribing a fixed particle size distribution for sedimentation and radiative effects (e.g. Timmreck et al., 1999; Oman et al., 2006; Aquila et al., 2012). However, size-resolved stratospheric aerosol modules which include microphysical processes such as new particle formation, coagulation and condensation have also been developed. The first Pinatubo aerosol microphysics simulations were carried out in two-dimensional models (Bekki and Pyle, 1994; Bekki et al., 1996; Weisenstein et al., 1997) with single-moment sectional schemes where mass in numerous size bins is transported. More recently, several 3-D general circulation models with aerosol microphysics schemes have also been used, to predict sedimentation and changes in radiative forcing in conjunction with the evolving stratospheric particle size distribution (e.g. Timmreck, 2001; Toohey et al., 2011; English et al., 2012, 2013).

Despite the diversity in model complexities, most of these studies evaluated their simulations against a limited set of observational data sets, primarily AODs derived using Advanced Very High Resolution Radiometer (AVHRR) and Stratospheric Aerosol and Gas Experiment (SAGE II) measurements. Using a mass-based prognostic stratospheric aerosol module in a middle-atmosphere version of the ECHAM4 climate model, Timmreck et al. (1999) showed that the two distinct maxima in AOD apparent in AVHRR and SAGE II based AOD could be simulated, but the model failed to simulate the observed slow AOD decay in the tropics after the peak. Similarly, using a low resolution composition-climate model coupled to an offline 3-D chemical transport model, Pitari and Mancini (2002) could simulate SH AOD reasonably well but their model simulated AOD were biased low in the tropics and NH. Aquila et al. (2012), presented results from a general circulation model coupled to a global aerosol transport model (using a mass-based aerosol scheme). However, they found that model simulated tropical AOD was higher than AVHRR or SAGE during ~~initial~~ few months, but showed very good agreement during er phase. Using a sectional aerosol microphysics module with injection altitude between 15.5 –27 km, English et al. (2013) achieved good agreement with SAGE and AVHRR observed AOD in NH mid-latitudes for the first 12 months after the

eruption but too rapid decay in AOD through later months. They also compared model aerosol effective radius (R_{eff}) evolution against observations from SAGE II and in-situ measurements (for e.g. Russell et al., 1996; Bauman et al., 2003), finding peak values in the model NH tropical stratosphere occurred earlier than in the observations. Some of these model-observation biases in earlier studies may be linked with the transport related issues (e.g. the lack of a Quasi-Biennial Oscillation, QBO) in the underlying GCM, whereas some may be linked to the simplified treatment of the particle size distribution. Other causes such as interactions with ash, or missing minor eruptions such as Mount Hudson in Chile (September 1991) have also been suggested.

Although they have near-global spatial extent, satellite measurements of AOD and R_{eff} constrain only integrated stratospheric aerosol properties over the full particle size range. Balloon-borne measurements (e.g. Deshler, 1994) enable a closer examination of the particle size distribution, but are available at only a small number of sites.

Here, we use both satellite and balloon-borne measurements to evaluate the UMUKCA simulated stratospheric aerosol properties, and seek to better understand the source of model biases. In Sect. 2 we describe the model, including the experimental set-up and the developments to the aerosol and chemistry schemes which extend its applicability to both stratospheric and tropospheric conditions. Section 3 describes the measurements that are used to evaluate the model. Results and discussion about potential causes of model-observation biases are presented in Sect. 4 and 5, respectively. Summary and major conclusions are presented in Sect. 6.

2 Model description

We use the stratospheric chemistry configuration of UMUKCA (Morgenstern et al., 2009) within the high-top version of the 3rd generation Hadley Centre Global Environmental Model (Hewitt et al., 2011) as used by Braesicke et al. (2013) and Telford et al. (2013). Although UKCA can be run with fully coupled aerosol-chemistry-dynamics with online radiative effects from the simulated aerosol, O_3 , CH_4 , N_2O and other gases,

here only the simulated O_3 is radiatively coupled. Sea-surface temperature and sea-ice fields are prescribed from the AMIP time-varying dataset (Hurrell et al., 2008). The simulations are carried out at N48 horizontal resolution (2.5° and 3.75° in latitude and longitude) with 60 vertical hybrid-height levels from the surface to 84 km.

In order to simulate stratospheric aerosol precursor gas phase species, we have extended the existing UKCA stratospheric chemistry scheme to also include sulphur chemistry (see Sect. 2.1). The coupling to the GLOMAP-mode aerosol microphysics module (Mann et al., 2010), and its adaptation for stratospheric conditions, is described in Sect. 2.2. Surface emissions of NO_x , CO and HCHO are from the RCP 4.5 scenario. Lower boundary conditions are applied for CH_4 , N_2O , CFC-11 ($CFCl_3$) and CFC-12 (CF_2Cl_2) according to WMO (2011). Heterogeneous chemical reactions use time-varying prescribed aerosol surface area density produced for the SPARC Assessment of the Stratospheric Aerosols Report (SPARC, 2006). We include surface and elevated emissions of anthropogenic SO_2 from Lamarque et al. (2010) with also a 3-D source from passively degassing volcanoes from Andres and Kasgnoc (1998). DMS emissions are determined by wind speed using a seawater concentration climatology of Kettle and Andreae (2000) with the sea-air exchange function of Liss and Merlivat (1986). We apply a fixed lower boundary condition of 275 pptv.

2.1 Stratospheric chemistry extended to include the sulphur cycle

The existing UMUKCA stratospheric chemistry scheme (Morgenstern et al., 2009) covers the oxidation of CH_4 and CO, with chlorine and bromine chemistry and their interaction with HO_x , NO_x and O_x cycles including heterogeneous reactions on polar stratospheric clouds (PSCs) and liquid sulfate aerosols (Chipperfield and Pyle, 1998). Here, we have extended the scheme to also include a stratospheric aerosol precursor chemistry scheme (Weisenstein et al., 1997) with updates to reaction rates from Sander et al. (2006), see Table 1. The added chemistry includes the steady background source of SO_2 from OCS, which principally maintains the stratospheric aerosol during volcanically quiescent periods (e.g. Carslaw and Kärcher, 2006). Also included

are photolysis reactions for H_2SO_4 and SO_3 , which occur above about 30 km and lead to a reservoir of SO_2 building up during polar winter, enabling new particle formation in polar spring (Mills et al., 2005). The chemistry is integrated with the ASAD chemical integration package (Carver et al., 1997) with the Newton-Raphson sparse matrix solver from Wild et al. (2000). Photolysis rates are calculated using the FAST-JX online photolysis (Neu et al., 2007) following the implementation described in Telford et al. (2013). The cross-section of H_2SO_4 is assumed analogous to the cross-section of HCl ($\times 0.016$) following the method of Bekki and Pyle (1992). Aqueous sulphate production in (tropospheric) liquid clouds is also passed to the GLOMAP module for growth of accumulation and coarse soluble particles.

2.2 The aerosol microphysics module adapted for the stratosphere

The GLOMAP aerosol microphysics module was developed as a component of the TOMCAT 3-D offline Chemical Transport Model (Chipperfield, 2006) with both 2-moment sectional (Spracklen et al., 2005) and 2-moment modal versions (Mann et al., 2010) available. The computationally faster modal scheme (GLOMAP-mode) was specifically designed for longer integrations within UМУKCA and applies the same aerosol microphysics representations as the sectional scheme but with the size distribution parameterised into 7 log-normal modes, being similar in framework to that used in ECHAM-HAM (e.g. Stier et al., 2005). The GLOMAP-mode scheme produces aerosol properties in good agreement with the more sophisticated sectional scheme under most tropospheric conditions (Mann et al., 2012).

Since this study investigates the evolution of the stratospheric aerosol layer after Pinatubo, we use only the four soluble modes and treat only sulphate and sea salt components, the latter included to give reasonable representation of tropospheric aerosol optical properties. For this work, the model approaches for water uptake, particle density, vapour condensation and new particle formation have been adapted to be applicable across stratospheric and tropospheric conditions. In the following subsections, we briefly describe these updates.

2.2.1 Water uptake

In the standard version of GLOMAP-mode described by Mann et al. (2010), water uptake is calculated using ZSR (Zdanovskii, 1948; Stokes and Robinson, 1966), which is not applicable in stratosphere conditions. At pressures below 150 hPa we therefore instead use the expression of Carslaw et al. (1995) to provide the aerosol water content. At 225 K and 101 hPa, the composition of the solution is 74.5 % H_2SO_4 and 25.5 % water, approximating the 75 % weight fraction assumed in some studies (e.g. Stenchikov et al., 1998; Oman et al., 2006).

2.2.2 Particle density

As composition of the aqueous sulphuric acid solution droplets also affects their density, we modified GLOMAP-mode for the stratosphere. For pressures lower than 150 hPa, density values for each mode are replaced with values from a look-up table based on the measurements of Martin et al. (2000) as a function of the sulphuric acid weight-fraction.

2.2.3 Condensation and vapour pressure of H_2SO_4

In all previous versions of the GLOMAP aerosol module, gas-to-particle transfer of H_2SO_4 occurs assuming zero vapour pressure, i.e. the transfer is represented as a condensation process. Although this approach is entirely appropriate in tropospheric conditions, above $\sim 25\text{--}30$ km, the vapour pressure of H_2SO_4 ($p_{\text{H}_2\text{SO}_4}$) becomes significant as the temperature increases in the stratosphere and above 35 km the sulphuric acid droplets rapidly evaporate (Hamill et al., 1997; Hommel et al., 2011).

We therefore now calculate $p_{\text{H}_2\text{SO}_4}$ online in the model following Kulmala and Laaksonen (1990) and calculate the condensation rate consistently with the difference between the vapour pressure and the gas phase partial pressure. We also apply a simple approach to particle evaporation whereby if the ambient gas phase H_2SO_4 par-

tial pressure is less than $p_{\text{H}_2\text{SO}_4}$, the number concentration for all modes is reduced at a fast decay rate of 50% per condensation timestep.

2.2.4 New particle formation

Previous versions of GLOMAP (e.g. Mann et al., 2010) formed new $\text{H}_2\text{SO}_4\text{-H}_2\text{O}$ particles based on the Kulmala et al. (1998) parameterization for binary homogeneous nucleation. This is only applicable at temperatures in the range 233–298 K. Vehkamäki et al. (2002) suggested that conditions for nucleation are also favourable at ~ 200 K in the upper tropical troposphere and they updated the Kulmala et al. (1998) parameterization to be applicable down to lower temperatures and humidities. To allow GLOMAP-mode to be applied in both tropospheric and stratospheric conditions, we have incorporated the Vehkamäki et al. (2002) parameterisation, and used it within the recommended ranges of temperature (190 to 305 K) and H_2SO_4 concentration (10^4 to 10^{11} cm^{-3}). Note that we also use the expression of Kerminen and Kulmala (2002) to convert the cluster nucleation rate from Vehkamäki et al. (2002) into an “apparent nucleation rate” at 3 nm. The nucleation rate is set to zero in subsaturated conditions.

2.2.5 Size distribution

Balloon-borne optical particle counter and condensation nucleus counter measurements in the mid-latitude stratosphere in the 1990s (e.g. Deshler et al., 2003) suggest a bimodal size distribution with the first mode at about 50–150 nm radius with σ_g between 1.6 and 1.8 and a larger much narrower mode ($\sigma_g \sim 1.2$) at around 300–800 nm radius that is weak in volcanically quiescent conditions but much stronger (in number) following the Pinatubo eruption (e.g. Carslaw and Kärcher, 2006). For example Deshler et al. (2003) show that in March 1993 (21 months after the Pinatubo eruption), in the NH mid-latitude lower stratosphere there was a 6 km layer (12–18 km) with the number concentration of particles with radii larger than 500 nm greater than 1 cm^{-3} . Such coarse particles have grown from their original size of around 1 nm due to coagulation

and gas-to-particle transfer of sulphuric acid. Modal microphysics schemes such as GLOMAP-mode represent this condensational and coagulative growth, but must use a technique referred to as “mode-merging” (e.g. Binkowski and Roselle, 2003) to transfer particles to adjacent larger modes following strong growth. In the case of a large volcanic eruption, the mode-merging may transfer particles first from the nucleation mode to the soluble Aitken mode, and following further growth up to the soluble accumulation mode and then to the soluble coarse mode. In each case, when particles are received from the adjacent smaller mode, the transferred number and mass is added to that existing in the mode, with the mean size re-formulated according to the prescribed standard deviation of the mode (σ_g).

Kokkola et al. (2009) compared size distributions simulated by a modal and three sectional schemes in a box model. While the four models agreed well in background stratospheric conditions, in volcanically perturbed conditions, the size distributions were found to be better represented with narrower mode widths. In particular, with the original coarse mode σ_g of 2.0, they found the modal scheme over-predicted the R_{eff} compared to a reference sectional scheme with a large number of bins. Niemeier et al. (2009) used an improved version of the same modal microphysics scheme whereby σ_g for the accumulation soluble mode was reduced to 1.2 and the coarse mode was de-activated.

Here we are applying the modal GLOMAP scheme to volcanically-perturbed stratospheric conditions, and also using the same modes to represent tropospheric aerosol. In the troposphere, the coarse soluble mode in GLOMAP-mode is almost exclusively containing sea-salt, and the scheme has followed Wilson et al. (2001) and Vignati et al. (2004) in using a value of 2.0 for σ_g in this mode, which are based on values given in D’Almeida et al. (1991).

To ensure the size distribution and vertical profile of the simulated coarse sea-salt particles is retained as evaluated in previous model versions (Mann et al., 2012), we retain the σ_g value of 2.0 for the coarse soluble. However, we now de-activate mode-merging between the accumulation and coarse soluble modes, which allows the accu-

5 mulation soluble mode to continue to grow larger than 1 micron diameter in strongly perturbed conditions. We also retain the σ_g value of 1.4 for the soluble accumulation mode in GLOMAP-mode, as reduced by Mann et al. (2012) from the value of 1.59 used in Mann et al. (2010) to better compare with size distributions simulated by the sectional scheme and from observations. The $\sigma_g=1.59$ values for the nucleation and Aitken modes are also retained.

2.3 Experimental setup

For this study, we carried out several 5-year model integrations, as summarised in Table 2. In addition to a background run (**C_noPinatubo**) without any Pinatubo emission, two reference simulations were carried out with 20 (**A_Control20**) and 10 Tg (**B_Control10**) of SO_2 injected into the tropical stratosphere on 15th June 1991 between 19 and 27 km. To ensure we closely match the initial spatial distribution of the aerosol cloud, we inject the SO_2 across the eight model grid boxes between $0-20^\circ$ N along 120.5° E. We emit 3% of the SO_2 mass from Pinatubo directly as sulphuric acid particles (assumed to form at the sub-grid scale) with half emitted with assumed geometric mean radius of 15 and 40 nm as in Spracklen et al. (2005). For all the simulations the entire set of tracers were initialised from fields after 8 years spin-up. The spin-up run started from zero aerosol and gas phase sulphur species, with other gases initialised from the UМУKCA REF-C1 integration from the SPARC Lifetimes Assessment Report (SPARC, 2013), representative of 1990 conditions.

To assess the robustness of the model to uncertainties in particle formation processes, which are known to be uncertain in the stratosphere, we also carried out two sensitivity simulations with are as run **B_Control10**, but we switch off the sub-grid particle source (primary sulphate emission) from Pinatubo (**B_Control10**) and reduce the nucleation rate (**E_ScaledStNuc10**) in the stratosphere by a factor of 2 (by multiplying it with 0.01).

3 Measurements

To evaluate the UKCA simulations, we use measurements from the SAGE II instrument (McCormick and Veiga, 1992), which was launched on the Earth Radiation Budget Satellite (ERBS) in 1984. SAGE II was a seven-channel Sun photometer operated in solar occultation mode with a vertical resolution of about 0.5 km. Spectral windows were centred at 385, 448, 453, 525, 600, 940 and 1020 nm. For evaluating the model stratospheric aerosol optical depth, we use the gap-filled SAGE-II (V6.2) product (Hamill et al., 2006) produced for ASAP (Assessment of Stratospheric Aerosol Properties SPARC, 2006). Simulated aerosol extinction is compared against the recently updated version (V7.0) of the SAGE-II data (Damadeo et al., 2013). We also compare to the SAGE-derived SAD product (Thomason et al., 1997) that is obtained from <http://www.sparc-climate.org/data-center/data-access/asap/>. Simulated SAD is also compared against the recently available SAD data Arfeuille et al. (2013) which was created using SAGE II V7.0 data, and is provided for the Chemistry Climate Model Initiative (CCMI) simulations. Further evaluation of the post-Pinatubo simulated aerosol optical depth (AOD) evolution was carried out by comparing to that measured by the Advanced Very High Resolution Radiometer (AVHRR/2), which was onboard on the National Oceanic and Atmospheric Administration (NOAA/11) satellite. For details see http://www.nsof.class.noaa.gov/release/data_available/avhrr/index.htm. The AVHRR instrument measures the reflectance of the Earth in five spectral bands centred around 0.6, 0.9, 3.5, 11 and 12 μm .

To examine the simulated particle size distribution that underpins the model aerosol optical properties, we also compare to profile measurements of size-resolved number concentration made at Laramie, USA (Deshler et al., 2003). The balloon-borne system includes a Condensation Nucleus Counter (CNC) to measure the concentrations of particles larger than 10 nm and an optical particle counter (OPC, Deshler et al., 1992) to measure size-resolved particle concentrations in several size ranges in the accumulation and coarse regions of the size spectrum. The OPC is a light counter

to derive integrated size distribution from measured aerosol scattering in the forward direction. The standard OPC design gives integral number concentrations larger than 150 nm and 250 nm radius, and has been used in balloon sounding measurements of ~~the~~ stratospheric aerosol since 1963 (Rosen, 1964), also giving important information about the stratospheric aerosol changes induced by the 1980 Mount St. Helen's eruption (Hofmann and Rosen, 1982). Deshler et al. (1992) present the measurements taken in the first few months after the June 1991 Pinatubo eruption, with most balloon flights using this original 2-channel OPC. An enhanced OPC, using an increased scattering angle, measured concentrations in 8 size channels for radii larger than 150 nm to around 10 microns. The 8-channel OPC had been developed shortly before the eruption, and became the default measuring system a few months after the eruption. The measurement capabilities were later further enhanced to measure up to twelve size ranges (see Deshler et al., 2003).

4 Results

Stratospheric aerosol sizes and concentrations are influenced by dynamical, chemical and microphysical processes. ~~For example background aerosol~~ are formed by homogeneous nucleation of H_2SO_4 and H_2O , with H_2SO_4 concentrations affected by oxidation of OCS and SO_2 . Microphysical processes such as nucleation, condensational growth, coagulation and sedimentation along with large-scale poleward transport determine lifetimes of these aerosol. To ensure the model is fully evaluated, it is necessary to evaluate the model against a range of aerosol properties, but it is also important to assess stratospheric circulation in the model and assess the evolution of key precursor gases which influence the aerosol.

4.1 Stratospheric dynamics in the UKCA

One of the most important factors controlling stratospheric aerosol is the stratospheric transport which is determined by the strength of the stratospheric Brewer-Dobson (BD) circulation. This circulation plays a crucial role in determining the evolution of the background as well as volcanically-enhanced stratospheric aerosol layer. Stronger BD circulation leads to rapid transport of air masses (and chemical species) from the tropics to high latitudes (e.g, Weber et al. 2003; Dhomse et al. 2006). This circulation also affects aerosol removal from the stratosphere (e.g. Deshler, 2008) via stratospheric-tropospheric exchange (STE, e.g. Holton et al. 1995). However, strength of the BD circulation is also coupled with the phases of quasi-biennial oscillation (QBO) via the Holton-Tan mechanism (Holton and Tan, 1980).

Using satellite observations, Trepte and Hitchman (1992) showed the importance of the QBO phase in determining the initial dispersion of the Pinatubo plume. So for the simulations presented here, the model is initialised such that the lower stratospheric winds are in the easterly phase of the QBO, as at the time of the eruption. Figure 1a shows the time evolution of the model monthly and zonal-mean zonal wind in the tropics (15°S – 15°N) against those from the ERA interim re-analysis from 1990 until 1995 (Fig. 1b Dee et al., 2011). As in ERA interim, the model begins an easterly QBO phase in mid 1991, although the model easterlies are weaker than in ERA-interim in the lower stratosphere for the first 6 months after the eruption. Also, the model easterly QBO phase begins slightly later than in ERA-interim, continuing until around September 1993 (at 30 hPa), compared to around January 1993 in the re-analysis. The semi-annual oscillation in the tropical middle and upper stratosphere is also well represented in the model.

A common metric used to assess stratospheric transport in chemistry-climate models (e.g. Strahan et al., 2011) is the mean stratospheric age of air. Figure 1c shows the latitude and altitude distribution of the model zonal-mean age-of-air (for 1991–2000) and Fig. 1d compares the model age of air at 50 hPa against that derived from air-

craft observations of the long-lived tropospheric source gases SF₆ and CO₂ (Hall et al., 1999). The values from other composition-climate models participating in the recent SPARC Lifetime Assessment (e.g. Chipperfield et al., 2014) are also shown for reference. In the tropics, the model age-of-air agrees well with the observations, but at mid- and high latitudes there is a low bias compared to the observations; up to one yr too young air at high latitudes. The low bias in mid-latitude age-of-air indicates that model may have too rapid meridional poleward transport and/or stronger STE. In turn, such a mixing can cause too fast removal of aerosol from the stratosphere into the mid-high latitude troposphere, and should be considered when drawing inference from the evaluation of the model post-Pinatubo stratospheric aerosol decay.

4.2 Global burden and e-folding timescale

Figure 2 shows the January 1991 to December 1994 time-evolution of the daily total global column mass burden of sulphur in the gas phase (as SO₂, red) and in the aerosol particle phase (blue) from runs **A_Control20** (solid line), run **B** (dashed line) and **C_noPinatubo** (dotted line). Separate lines indicating the upper tropospheric and stratosphere (UTS) aerosol sulphur burden (above 400 hPa, green lines) and that in the lower-middle troposphere (below 400 hPa, aqua lines) are also shown. From the no-Pinatubo run **C_noPinatubo**, the global SO₂ and aerosol sulphur burdens are mostly in the troposphere, and their timeseries are dominated by anthropogenic emission sources, which are mainly in NH mid-latitudes. Photochemistry is strongest during summer, with higher oxidants then causing efficient conversion of SO₂ to aerosol sulphate. Only 10 % of this background total sulphur burden is in the form of SO₂ during the NH summer, compared to around 50 % during winter. We find 30–40 % of the total aerosol sulphur burden (around 0.5 Tg S) is in the stratosphere, which is considerably higher than the 17 % (0.15 Tg S) found by Hommel et al. (2011). Tropospheric aerosol burdens are also higher than other models (e.g. Textor et al., 2006) at around 1.25 Tg S on the annual mean.

For run **A_Control20**, the global column SO₂ burden decays from an immediate post-

eruption peak of 10.3 Tg to around 2.0 Tg SO₂ burden on day 226 (60 days after the eruption). Subtracting the 0.3 Tg SO₂ mass from **B_Control10** (which is all in the troposphere), gives 1.7 Tg S, suggesting 8.3 of the emitted 10 Tg S emitted as SO₂ has been chemically converted to sulphuric acid over that period. We therefore estimate the e-folding timescale for conversion of SO₂ into sulphuric acid aerosol as 60 divided by $\ln(10/1.7)$ which is 35 days, which agrees closely with most previous studies. For example Bluth et al. (1992) derived an e-folding timescale of 35 days from the TOMS satellite SO₂ measurements, but present this as a tentative estimate. McCormick and Veiga (1992) derived an approximate aerosol sulphur burden assuming a 50% conversion from SO₂ to H₂SO₄ by the end of July, which corresponds to an e-folding timescale of 43 days. Oman et al. (2006) found an SO₂ e-folding conversion timescale of 35 days in their model, which used fixed OH concentrations. We note however in the first month of the eruption there is much slower conversion to aerosol of the volcanic emitted SO₂, compared to the timescale over 60 days. For example, at day 200 (34 days after the eruption) there is 5.6 Tg of sulphur in the form of SO₂, which gives an e-folding timescale of 59 days. Bekki (1995) found that oxidant concentrations can be strongly depleted after very large volcanic eruptions, and in their simulation of Pinatubo Bekki and Pyle (1994), found a timescale of 40 days.

In Figure 2, we also show the timeseries of stratospheric aerosol sulphur burden derived from HIRS measurements by Baran and Foot (1994). For run **A_Control20**, we find the peak in global aerosol sulphur burden occurs 3 months after the eruption in September, in agreement with the timing derived from HIRS. However, the stratospheric aerosol sulphur burden from **A_Control20** is much higher than the observations, with a maximum of 9.3 Tg of sulphur (37 Tg aerosol mass assuming 75% sulphuric acid composition), substantially higher than the 5.4 Tg of sulphur (21.6 Tg of aerosol) from Baran and Foot (1994). Based on ISAMS measurements, Lambert et al. (1993) estimated the post-Pinatubo peak stratospheric aerosol burden between 19 to 26 Tg (4.75 to 6.5 Tg of sulphur). Since **A_Control20** gives much too much sulphur in the stratospheric aerosol compared to both of these estimates, we carried out a second

control simulation, **B_Control10** with 10 Tg of SO₂ (dashed line in Figure 2).

The stratospheric aerosol sulphur burden from **B_Control10** is in good agreement to the values derived from HIRS through the second half of 1991 and the whole of 1992. However, the HIRS measurements suggest a return to approximately background stratospheric aerosol levels by the middle of 1993, the model aerosol shows much slower decay, even showing modest enhancement at the end of 1994. Also, **A_Control20** has a peak stratospheric aerosol burden of 9.3 Tg at around day 260, but the aerosol burden from **B_Control10** peaks around a month earlier, at around day 230, with 5.25 Tg of sulphur. For **A_Control20** and **B_Control10**, we find around 6.1 Tg and 3.5 Tg of sulphur by June 1992 (12 months after the eruption, day 530), suggesting e-folding timescales of 19 and 24 months, respectively. The shorter removal timescale for the 20 Tg run is likely due to the particles growing to larger sizes compared to the 10 Tg run (e.g. as seen in Figure 8), and therefore sedimenting faster, moving to altitudes closer to the tropopause, where removal from the stratosphere is more effective. We note that both of these timescale estimates are considerably longer than estimates in the literature which range from around 12 to 14 months (e.g. see Baran and Foot, 1994 and Bluth et al., 1997).

4.3 Perturbation in sulphur species

Figure 3 shows vertical profiles of mixing ratios of the three key gas phase sulphur species OCS, SO₂, H₂SO₄, and of sulphuric acid in the particle phase (P-H₂SO₄), from runs **A_Control20** and **C_noPinatubo**. The left and right panels are for mean profiles in the tropics (20° S–20° N) and NH mid-latitudes (35–60° N), respectively with the top and bottom rows indicating the means for July 1991 and October 1991, selected to correspond to the 15–45 day post-eruption period when the SO₂ is oxidised to H₂SO₄ vapour, and approximately when the peak global aerosol burden occurs in the model. The profile of OCS shows the expected shape, being constant in the troposphere and then reducing with increasing altitude in the stratosphere as it is photolysed. The SO₂ profile from run **C_noPinatubo** shows a sharp reduction with height across the

tropopause but then reaches a minimum and begins to increase with height to a local maximum at 30 km corresponding to where the source from OCS photolysis is largest. Below 30 km the sulphuric acid vapour follows a similar shape as SO₂ (but at lower concentrations) but above that altitude continues to increase up to about 40 km. Below 35 km, the vertical profile of P-H₂SO₄ is approximately constant in the tropics in these quiescent conditions, but has a slight decrease with altitude. In the upper-middle stratosphere rapidly evaporating particles release their H₂SO₄ to the gas phase causing a sharp reduction in P-H₂SO₄ around 40 km.

In the tropics, the July profiles from run **A_Control20** (Fig. 3a) show large changes in concentrations of SO₂ and P-H₂SO₄ (between 20 and 30 km) relative to run **C_noPinatubo** increasing by factors 10³–10⁴ and factor 10², respectively. The enhanced P-H₂SO₄ profile indicates that much of the SO₂ has already been oxidised and condensed into the particle phase. By contrast, the NH mid-latitude July profiles shows that the Pinatubo plume has not yet been transported with SO₂ and aerosol H₂SO₄ still at quiescent concentrations over almost the entire stratosphere, although some perturbation can be observed in the lowermost stratosphere and uppermost troposphere. It is notable that balloon-borne particle concentration soundings at Laramie (41° N) in July 1991 already show some enhanced layers between 15–18 km (Deshler et al., 1992) which corresponds well with the altitude of the SO₂ and P-H₂SO₄ enhancement seen in the July-mean NH mid-latitude profiles. However, it is also important to note that the lower stratospheric observed aerosol enhancement in July 1991 at Laramie and Garmisch has been associated with a small eruption on June 12 which also injected some material directly in to the stratosphere (Jäger, 1992; Deshler et al., 1993).

The October mean SO₂ profile is still strongly enhanced (factor 100) in the tropics with the P-H₂SO₄ enhancement only slightly higher than in July but over a much deeper layer. This tropical enhancement in both SO₂ and P-H₂SO₄ propagates up to about 40 km, and above that only the SO₂ profile show differences between runs **A_Control20** and **C_noPinatubo**. It is interesting that the October 1991 tropical gas phase H₂SO₄ profile from run **A_Control20** actually shows lower values than in run

C_noPinatubo in the main part of the plume (15–30 km), due to the condensation sink to aerosol being so much stronger. By contrast above 30 km the increase in vapour pressure shuts off the condensation sink leading to the H₂SO₄ vapour concentrations being higher than quiescent at those altitudes. The October 1991 NH mid-latitude SO₂ and P-H₂SO₄ profiles show only moderate enhancement suggesting the easterly phase of the QBO has prevented transport of Pinatubo-enhanced air masses.

4.4 Aerosol optical depth (AOD) comparison

Figures 4a and b show the time evolution of the model mid-visible stratospheric AOD from runs **A_Control20** and **B_Control10** while Figures 4c and d show the mid-visible AOD measured from SAGE II and AVHRR. Since AVHRR is a nadir viewing instrument, in Fig. 4d we have subtracted monthly-mean AODs for the year prior to the eruption, matching the procedure recommended by Long and Stowe (1994) and used by Aquila et al. (2012). Note that the SAGE-II derived AOD is much lower than AVHRR in the tropics during the very high loading period after Pinatubo due to the measured extinction saturating (Hamill et al., 2006). In both the **A_Control20** and **B_Control10** runs there is good qualitative agreement with the satellite regarding spatial and temporal distribution. For example, there is high AOD after the eruption centred around the equator with peak AOD in September 1991 in both model simulations and in the two satellite datasets. However, the model feature is narrower, confined between 10° N and 10° S. Another well-captured feature in the model is that there is no significant enhancement of AOD in NH mid-high latitudes until October 1991.

However, consistent with Fig. 2 (more aerosol loading than estimated by Baran and Foot (1994)) the simulated AOD in **A_Control20** is much larger than both sets of observations. The AOD distribution in **B_Control10** is in better agreement with the satellite measurements, comparing well to both satellite measurements in mid- and high latitudes. Comparing to the observed AOD enhancements in the SH, both model simulations are also in quite good qualitative agreement. However, in the tropics the AOD in **B_Control10** is still about 50% larger than that derived from AVHRR, and a

factor two larger than SAGE-II. Possible causes for these ~~higher~~ biases are discussed later in this section.

4.5 Extinction comparison

Extinction profile measurements from SAGE-II between July and September show (e.g. McCormick et al., 1995) that transport to the SH occurred mostly above about 24 km altitude. Aquila et al. (2012) highlighted the importance of resolving the enhanced tropical upwelling which occurred due to the long-wave absorption by the relatively larger stratospheric aerosol after the Pinatubo eruption. As explained in Sect. 2, in these simulations we do not radiatively couple the simulated aerosol with the model dynamics, and yet we capture quite well the SH post-Pinatubo AOD evolution. We note that Aquila et al. (2012) do not include evaporation of sulphuric acid in their model, which could play an important role in influencing transport to SH mid-latitudes.

Figure 5 shows a timeseries of aerosol extinction from three model simulations (runs **A_Control20**, **B_Control10**, **C_noPinatubo**) and SAGE-II at 32, 25 and 20 km in the tropics (20° S–20° N). We choose these altitudes to allow comparison with the evaluation presented in Weisenstein et al. (2006, Fig. 6.20) for other stratospheric aerosol models. We compare extinction in the mid-visible (left panels) as well as the near infrared (right panels). Here we use the updated v7.0 SAGE-II dataset and the profiles shown are averages between 20° S and 20° N. Monthly mean observed values are calculated based on both sunrise and sunset profiles.

At 20 and 25 km, both runs (**A_Control20** and **B_Control10**) capture the general evolution of the tropical mid-visible extinction (Figure 5), with the magnitude and timing of peak values, and the decay timescale, agreeing well with SAGE-II. However, before the eruption (background conditions), modelled extinctions have a moderate low bias of 20–50 % at these levels. For the tropical mid-visible extinction timeseries, run **B_Control10** is in better agreement with the observations than **A_Control20**, which tends to be high biased (consistent with the AOD and aerosol mass high biases seen in Figures 2 and 4 respectively). However, against the tropical near infra-red extinc-

tion, run **A_Control20** is in better agreement, with run **B_Control10** generally showing modest low bias, although still in reasonable agreement. At 25 km, the model tropical extinction peaks in August 1991, whereas in the satellite measurements, values plateau for 2–3 months before the decay period begins. In the model, the decay is fastest in the first 6–8 months after the peak value, with an approximately constant e-folding timescale from mid 1992 onwards. The faster decay in the initial period is likely reflecting the shift in size distribution as larger particles are removed earlier in the period, causing slower sedimentation rates afterwards. Larger model high bias is seen for simulated tropical extinctions at 32 km, for both the runs (**A_Control20** and **B_Control10**) that may indicate that the upper altitude used for SO₂ injection was too high. At 32 km, the modelled extinction is slightly larger than SAGE-II and, although peaks and troughs are mostly similar to the satellite measurements, the model variability is less than in the observations. We note again that our model does not include the dynamical effects of aerosol-induced radiative heating. Such a radiative heating is known to cause increased tropical upwelling, which would cause greater dilution, could alter horizontal transport through the subtropical barrier and may also alter microphysical processes such as evaporation.

Figure 6 shows a similar analysis to Fig. 5, but for NH mid-latitudes (35–60° N), again to compare against models shown in Weisenstein et al. (2006). At 20 km, there is very good agreement between modelled and SAGE II extinctions at both mid-visible and near near-infrared wavelengths. Similar agreement is observed at 25 km however, during 1993 SAGE II measurements show a significant decrease at both wavelengths which is not captured by the model. At 32 km the modelled extinction enhancement is slightly larger than the observations. We also note that whereas in the tropics the model and observations showed a faster decay phase in the first 6–8 months after the peak aerosol loading compared to the later phase, in NH mid-latitudes, both model and observations have constant exponential decay timescale throughout the post-eruption period. Overall at this latitude band, the model shows much better agreement with SAGE II measurements compared to the models that participated in SPARC (2006). Inter-

estingly, differences between runs **A_Control20** and **B_Control10** are much smaller at this latitude band than in the tropics (Fig. 5), suggesting a larger proportion of aerosol is removed in the tropics in the 20 T_g run (likely related to stronger sedimentation). Again as in the tropics, at 20 km, the ~~1020~~ km extinction from run **B_Control10** shows better agreement with SAGE II than in **A_Control20**.

4.6 Surface area density (SAD) comparison

Figure 7 compares the vertical and latitudinal distribution of zonal mean SAD from run **A_Control20** against two versions of the satellite-derived SAD dataset, for four selected months between May 1991 and May 1992. Before the eruption (May 1991), the model captures the observed SAD very well with a hemispherically symmetric distribution in the lower stratosphere in the range 0.5 to 2 $\mu\text{m}^2\text{cm}^{-3}$. For September 1991 (three months after the eruption), although the simulated SAD distribution broadly matches the observed shape, it is up to a factor 2 to 3 too high in the tropics. Also, the model Pinatubo-enhanced SAD plume is too strongly confined to the tropical pipe, whereas in the satellite-derived SAD (Fig. 7d) one can see weak meridional transport to NH and SH sub-tropics at about 20–22 km. Young et al. (1994) showed that including the aerosol radiative effects on the model dynamics broadens the latitudinal extent of the Pinatubo cloud, thus improving agreement against the satellite observations. And as mentioned earlier such a heating can alter local circulation and may partially explain the SAD high biases seen here. By January 1992, the model high bias has reduced to a factor of 2, and the model shows meridional transport to NH mid-latitudes in the lowermost stratosphere, also seen in the observations. However, the satellite-derived SAD suggests meridional transport also occurs to the SH, but at slightly higher altitudes. By May 1992, high biases in modelled SAD are much smaller and the general latitudinal and altitudinal distribution is still in good qualitative agreement with the observations, aside from the continued low bias in the SH. Also, as observed in Figure 2 (younger age-of-air), in the lowermost stratosphere, the model seems to have too much diffusion near the tropopause. Hence the distinct cross-tropopause gradients seen in satellite

data are not seen in our simulations.

While interpreting the model-observation SAD discrepancies, one should consider how the satellite SAD product is derived from the SAGE I, SAGE II, SAM II (Stratospheric Aerosol Instrument II) and SME (Solar Mesosphere Explorer) measurements.

5 As noted earlier, the extinction measured by the SAGE and SAM instruments has an upper limit of 0.01 km^{-1} , above which the atmosphere is effectively opaque to the instruments (Hamill et al., 2006). During the peak aerosol loading period, when the model SAD is a factor of 2 high biased, it is apparent (for example in Fig. 5) that the SAGE II 525 nm and 1020 nm extinctions in the tropical lower stratosphere are saturat-
10 ing at the upper limit value, with actual extinction values likely to have been higher. The late-1991 to 1992 period was flagged as missing data in the original SAGE-II extinction dataset. The data gaps during that period were addressed by Hamill et al. (2006), who used lidar data from two tropical sites (Camaguey, Cuba and Mauna Loa, Hawaii) and two mid-latitude sites (Virginia, USA and Lauder, New Zealand), to fill the missing data.

15 Another important issue to consider with the SAGE-II derived SAD product is that, even outside the gap-filled part of the dataset, particles smaller than 50 nm are essentially invisible to the satellite and there is little sensitivity to particles smaller than 100 nm. Reeves et al. (2008) derived extinction, SAD and volume concentration from aircraft measurements of the aerosol particle size distribution (in quiescent conditions)
20 and compared to SAGE-II products. They found the aircraft measured SAD was a factor 1.5–3 higher than the SAGE-II derived values, whereas volume concentrations were only 35 % higher.

4.7 Effective radius (R_{eff}) comparison

Another product derived from the gap-filled satellite extinction record, that can be used to assess the evolution of the stratospheric aerosol properties following the Pinatubo eruption, is the R_{eff} , defined as the ratio of the 3rd and 2nd integral moments in radius

and for multimodal distribution can be represented as (Russell et al., 1996, Eq. 6):

$$R_{\text{eff}} = \frac{\sum_{i=1}^m N_i r_{gi}^3 \exp [9/2(\ln \sigma_i)^2]}{\sum_{i=1}^m N_i r_{gi}^2 \exp [2(\ln \sigma_i)^2]} \quad (1)$$

The two gap-filled SAGE/SAM extinction data products thereby provide 3-D time-varying volume concentration and SAD which together give R_{eff} throughout the Pinatubo period. This record therefore has the potential to give information on how the particle size distribution in the stratosphere was perturbed by the eruption. However, again, when comparing the model to the satellite R_{eff} , the limitations associated with the derived product need to be considered. In particular, because of the “blind spot” associated with particles smaller than 50–100 nm, Hamill et al. (2006) state that since the derived SAD may have an inherent low bias (whereas the derived volume density will be less affected) the derived R_{eff} may overestimate the true value.

Figure 8 shows the evolution of the model zonal-mean R_{eff} at 20 and 25 km from runs **A_Control20** and **B_Control10** compared to that derived by Bauman et al. (2003) from the SAGE-II and CLAES satellite measurements. The general spatial and temporal evolution of the model R_{eff} is in good qualitative agreement with the observations in both runs, with values at 20 km larger than at 25 km, likely due to sedimentation. In the tropics, at both altitudes, the observations suggest that, whereas AOD and extinction are decaying by November or December 1991 (Figures 4 and 5), the effective radius peaks several months later (early 1992) with only a slow decay beginning later in 1992. By contrast, in NH mid-latitudes, the observations suggest the decay in effective radius is slightly earlier and occurs faster. Both simulations capture the timing of these R_{eff} peaks well, although at 25 km, the model peak is later than observed, matching the timing at 20 km. Effective radius values are always higher in the tropics than at mid-latitudes, a feature that is consistent between the model and observations. However, although R_{eff} from run **A_Control20** are slightly larger than **B_Control10**, modelled values are up to 30–40% lesser than those derived from the satellite, with maximum model R_{eff} of around 0.4 and 0.35 μm , compared to around 0.6 μm from the satellites.

At 20 km (Fig. 8b), despite combining the two sets of satellite products, there is no observational constraint on the tropical R_{eff} between approximately June 1991 and August 1992, but the overall shape suggests the R_{eff} was likely even larger than $0.6 \mu\text{m}$ during that period. The model low bias in R_{eff} is apparent at about the same extent at all latitudes and altitudes and before the eruption, which suggests it is not associated with sedimentation, since that would be expected to occur mostly during the highest loading period. There appears to be a more persistent bias in simulated particle size distribution, but it is unclear whether the model has too many small particles, or too few large particles.

4.8 Particle size distribution

To give a stronger observational constraint on the simulated size distribution, we compare the model against balloon-borne CNC and OPC measurements made at Laramie, Wyoming, USA (41°N , see Sect. 3). Figures 9 and 10 compare model profiles of size-resolved number concentrations (larger than a given particle diameter) against those measured by the CNC and OPC. In each case we are comparing a monthly-mean size-resolved particle concentration to a single balloon sounding. Note that whereas the number concentration profiles for particles larger than 5 nm, 150 nm and 250 nm are exactly as measured by the OPC, for the larger size channels we have interpolated the observations (linearly in $\log N$ vs. $\log R$ space) onto regular $D_p > 550 \text{ nm}$, 750 nm and 1000 nm size channels from the irregular size thresholds given in the individual sounding data files.

Figure 9 shows the observed (plus signs) profile evolution of the particle size distribution through August to November 1991, for the period after the Pinatubo plume was first detected at Laramie on 16 July (Deshler et al., 1992). In August and September 1991, both runs **A_Control20** and **B_Control10**, show elevated values of N_5 , N_{150} and N_{250} between 14 and 20 km, whereas at higher altitudes (above 25 km) the profile remains close to background values (not shown). The region with elevated N_5 , N_{150} and N_{250} profiles matches reasonably well with the observations, and indicates efficient transport

of air from the tropics in the lowermost stratosphere. However above 25 km the model is not able to simulate steeper decreases observed in vertical profiles of N_{150} and N_{250} . Intriguingly, in November 1991 (Figure 9d) run **A_Control20** predicts only slightly higher N_{150} and N_{250} than run **B_Control10**, with particle concentrations at larger sizes showing a much larger relative enhancement in the 20 Tg run than the 10 Tg run. The size distribution simulated by the model is generally in good agreement with the observations, although in August and September 1991, near 20 km modelled particles larger than N_{550} are low biased compared to the observations, and there is a general over prediction of N_{10} in this initial post-eruption phase. The low bias in the larger sizes could be related to the high bias in the smallest sizes, with the condensation sink being shared out across a larger number of particles leading to reduced particle growth. Another possibility is that there is faster stratosphere-troposphere exchange as observed in the age-of-air comparison (Figs. 1c and 1d). Observations also show approximately nearly constant N_5 between 20 and 30 km, but run **A_Control20** (**B_Control10**) shows a slight increase (decrease) near 20 km and a steady decrease (increase) up to 25 km. The observations show that concentrations of particles at 150 nm and larger reduce sharply above 32 km, whereas the model profiles show only moderate decline. This may be indicating that the simple approach to particle evaporation in the **model is too slow.**

For November 1991, the run **A_Control20** shows enhancement up to 25 km for all the particle size thresholds, with the coarse mode higher than the run **C_noPinatubo** in the lowermost stratosphere (not shown), in good agreement with the observations. The model also shows an enhanced layer of N_5 , N_{150} and N_{250} at about 35km, suggesting transport of the Pinatubo plume to mid-latitudes throughout the lower and middle stratosphere. In both the model and observations, in these initial months, there is a layer where the N_5 and N_{150} lines come together, reflecting that few particles remain smaller than 150 nm and indicating that particle growth at these sizes is strongest in that part of the stratosphere. We note however that in the observations this confluence occurs at around 20 km, whereas in the model this occurs around 16-17km. This

discrepancy in altitude could be related to transport deficiencies in the model, and the general good qualitative agreement with the observations suggests that the modal approach to aerosol dynamics is capturing the evolution of the size distribution rather well.

5 In order to evaluate the model size distribution profile in quiescent conditions, we compare to the Laramie balloon measurements in March 1991 (Fig. 10a). We then probe the longer-timescale evolution of the size distribution through the Pinatubo period, in March 1992, 1993 and 1994 (Fig. 10b, c and d). Before the eruption, the observations show that N_5 decreases with increasing altitude between 12 and 23 km, whereas N_{150} and N_{250} show very little decrease with height. This feature is well captured by the model with N_5 and N_{150} in excellent agreement with the observations in this altitude range, although N_{250} has a slight low bias. Between 25 and 30 km, the observed N_5 profile shows a layer of enhanced concentrations, by around a factor of 10 compared to a continuation of the decrease seen at lower altitudes. This layer indicates a source of freshly nucleated particles which have not yet had time to grow to larger sizes. The simulated N_5 profile also shows this feature, but the enhancement of particle concentrations is much stronger in the model, and extends to lower altitudes, down to around 20km. Gas phase sulphuric acid concentrations are known to increase rapidly with height in this region from balloon-borne ion mass spectrometer measurements (e.g. Arnold et al., 1981). These elevated concentrations of gas phase H_2SO_4 have been shown to cause significant nucleation in the middle-stratosphere (Hommel et al., 2011) which is almost certainly the cause of this feature. The high bias in the model N_5 profile in this enhanced layer likely indicates that nucleation is too strong in the model. The over-predicted nucleation rate in these volcanically quiescent conditions may be a result of gas phase concentrations of H_2SO_4 being too high in the model. One possible explanation might be a lack of meteoric debris as a sink for gas phase H_2SO_4 suggested by Saunders et al. (2012) and Brühl et al. (2013) or weaker H_2SO_4 photo-dissociation.

25 In March 1992 (Fig. 10b), 9 months after the eruption, the observed particle con-

centration profiles show major enhancements throughout the upper troposphere and lower stratosphere (10 to 25 km), for size channels 150 nm and larger. By contrast, N_5 shows a slight increase compared to March 1991, and is only marginally higher than N_{150} and N_{250} for this month, suggesting that a large proportion of the particles have grown to sizes larger than 250 nm. The enhanced profiles of N_{550} , N_{750} and N_{1000} are approximately constant in altitude between 15 and 20 km with a fast decrease above 20 km. Model run **A_Control20** (solid line) captures this volcanically enhanced particle size distribution remarkably well, with good qualitative and quantitative agreement across all the size channels in the main part of the plume. Run **B_Control10** (dashed line) also captures well the N_5 , N_{150} and N_{250} profiles, but is low biased in the larger size channels. Despite generally very good agreement with the Laramie OPC data at this time, in the lowermost stratosphere and upper troposphere (between 10 and 15 km), both model runs show a high bias in N_{150} and N_{250} . We saw from the previous comparisons that run **A_Control20** has too high a burden in the stratospheric aerosol compared to the HIRS and ISAMS satellite measurements (Figure 2) and that it is strongly biased high in aerosol optical depth against the SAGE-II and AVHRR data (Figure 4). The comparisons to the OPC data suggest the high AOD bias originates from the overpredicted particle concentrations in the 150 to 550 nm radius range in the lowermost stratosphere, with coarser particles in that part of the atmosphere in reasonable agreement (run **A_Control20**) or showing low bias (run **B_Control10**). It is worth noting that in radiatively coupled simulations, we expect increased tropical upwelling would dilute the lower part of the plume, decreasing particle concentrations in the lowermost stratosphere.

In March 1993 (Fig. 10c), the observations show clear separation between N_5 and N_{150} , although N_{150} and N_{250} are close together. This indicates the formation of a bimodal size distribution consisting of an external mixture of particles which have grown to larger sizes following oxidation of volcanic SO_2 and a separate sub-population of particles less influenced by the eruption. Observed profiles of N_{550} , N_{750} and N_{1000} show peak values at around 12 km at this time, much lower altitudes than at March 1992

(Fig. 10b). It is interesting that the March 1993 N_{550} and N_{750km} profiles are higher in the 10-15km region than in March 1992, likely indicating the slow particle sedimentation at these particle sizes. The model captures the observed size distribution fairly well, with N_{250} in quite good agreement with the measurements. However, the model N_{150} profile has a high bias of around a factor of two, still being together with the N_5 profile between 15 and 20km. Also, simulated particle concentrations in the larger size channels have a strong low bias of around a factor of 10 (run **A_Control20**) or 20 (run **B_Control10**) in the lowermost stratosphere at this time, with the simulated profiles not capturing the increase in particles larger than N_{550} in the lowermost stratosphere.

By March 1994 (Fig. 10d) the OPC measurements show that there has been a general decay in all size channels towards background conditions. The model N_{150} high bias seen in March 1993 has worsened with the decay rate at these channels slower than in the observations. In the N_{550} , N_{750} and N_{1000} channels, the model continues to have a low bias in both simulations. It is notable that throughout the period, the model N_{150} and N_{250} profiles are remarkably similar between the **A_Control20** and **B_Control10** simulations, with much larger differences in the coarser sized particles.

5 Discussion

The comparisons against the balloon measurements (Figs. 9 and 10) show that the model captures well the general evolution of the particle size distribution in the stratosphere through the Pinatubo period. The observations indicate how the huge injection of SO_2 led after the eruption to the growth of some particles to sizes larger than $1 \mu\text{m}$ at peak loading (e.g. Figure 10b), with a long-lasting perturbation to concentrations larger than 150 nm with a complex evolution of R_{eff} (Fig. 8). The shift in the size distribution to a larger R_{eff} will have caused significant changes in the radiative properties of the stratospheric aerosol, with significant absorption of outgoing terrestrial radiation and a decrease in the efficiency of back-scattering of incoming solar radiation. These altered radiative effects illustrate the importance of resolving aerosol particle

size changes and subsequent feedback on dynamics in stratospheric composition-climate models, and we aim to include and assess the impact of these feedback in a future study (Mann et al., in prep., 2014).

Our simulations here indicate that the model is capable of capturing the main features of the observed evolution of the particle size distribution ~~very~~ well, with particularly good agreement with the measurements in the most perturbed post-eruption period through to mid 1992. However, Figure 10c and d suggest that the decay phase is not well captured, with N_{150} reducing much more slowly than the measurements and the return to a background size distribution occurs much later in the model. We have seen that simulated particle concentrations in the 5–250 nm size range, whilst agreeing well in background conditions, have moderate high bias in the first year after the eruption, with the bias worsening as the model decays too slowly in the subsequent period. There are several possible causes for this model size distribution bias. It could be that the simplified modal representation of aerosol dynamics may be only partly capturing the different particle growth and removal rates across the particle size range. However it is also worth noting that the largest biases occurred in the lowermost stratosphere and upper troposphere where stratosphere-troposphere exchange processes may not be well captured in our low resolution GCM. Another related issue is that we again note that these simulations do not include the coupling to dynamics which would increase the altitude of the aerosol layer and reduce concentrations in the lower part of the plume, where the high bias is mostly evident. Also, our model has too young age-of-air in mid-latitudes (see Figure 1d) which may also be affecting the simulated transport and particle size evolution. Finally, we also note that nucleation rates at the very low humidity and temperature conditions in the stratosphere are known to be highly uncertain. The Vehkamäki et al. (2002) parameterization used in this paper is the best available for stratospheric conditions, but is essentially an extrapolation from laboratory measurements at much higher temperatures and humidities, based on classical nucleation theory.

Our study is the first to fully examine the variation in simulated particle size dis-

tribution through the Pinatubo eruption, and we therefore choose to document the nucleation rate occurring in our simulations. Fig. 11 shows, for runs **A_Control20**, **B_Control10** and **C_noPinatubo**, the zonal-mean nucleation rate against latitude and altitude for monthly means through August to October 1991. In volcanically quiescent conditions (**C_noPinatubo**), the model has nucleation occurring mainly in the tropical upper troposphere with negligible new particle formation in the stratosphere. Note that the observed and simulated lower stratospheric N_5 and N_{150} profiles at Laramie in March 1991 (Fig. 10a) are in very good agreement, and Fig. 11 indicates that these stratospheric particles were actually formed in the tropical upper troposphere, consistent with the stratospheric aerosol lifecycle described by Hamill et al. (1997). The observations at Laramie indicate that only a small proportion of these nucleated particles grow to sizes larger than 150 nm, with most being at smaller sizes. We note however that nucleation can be seen in SH mid-latitudes in the volcanically quiescent **C_noPinatubo** September 1991 monthly-mean, indicating the occurrence of nucleation in springtime, as seen in the McMurdo OPC record, (Campbell and Deshler, 2014). Note that the mechanism here is that particle evaporation and subsequent photolysis of sulphuric acid leads to a reservoir of SO_2 building up during polar winter, which leads to new particle formation in polar spring (Mills et al., 2005). This is the same mechanism that is leading to the layer of elevated N_5 at 25-30km in the March Laramie profiles (see Figure 10).

Following the eruption of Mount Pinatubo, the balloon observations at Laramie indicate that, by March 1992 (e.g. Figure 10b), N_{150} is increased by a factor of 8, whereas N_5 has already returned to pre-eruption values. As a consequence, the N_5 and N_{150} profiles are separated by only a few tens of percent, indicating the majority of particles in the lower stratosphere have grown larger than 150 nm at that time. This feature was well captured by the model in runs **A_Control20** and **B_Control10** with the N_5 , N_{150} and N_{250} profiles being remarkably similar between the two runs. Figure 11 suggests that, following Pinatubo, strong nucleation occurred throughout the injection height range of 19–27 km for around 6 weeks after the eruption. Nucle-

ation rates then reduce in magnitude through August and September as the emitted SO_2 is completely converted to sulphuric acid and there is a substantial surface area to provide a condensation sink of H_2SO_4 . By October 1991, nucleation rates in **A_Control20** and **B_Control10** have returned to similar values to those found in the quiescent **C_noPinatubo** simulation.

Since uptake of reactive gases is dependent on particle size, accounting for the shift in size distribution may also be important for better quantification of the influence that volcanically enhanced aerosol has on stratospheric ozone through accelerated heterogeneous chemistry. We therefore investigate the evolution of the SAD distribution across the 3 stratospheric aerosol modes (Fig. 12) from July 1991, 15 to 45 days after the eruption (panels a to d) and in October 1991, when aerosol loading was close to its peak (panels e to h). Nucleation mode particles are always smaller than 10 nm, so even during July 1991, when substantial nucleation is occurring (Fig. 11) their contribution to total SAD is at most only around 10%. However, although the Aitken mode particles are smaller than 100 nm, during the early part of the eruption they contribute significantly to SAD in the upper part of the plume (28 to 30km). However, the accumulation mode SAD fraction (Figure 12 c) shows that even during early phase of eruption total SAD is primarily determined by these larger particles in lower-middle stratosphere. At a later stage (December 1991, not shown), the contribution from nucleation and Aitken mode is insignificant and as expected, the accumulation mode then contributes the vast majority of the SAD. We note that in Fig. 7 the model shows highest biases in simulated SAD against the observations during the first few months after the eruption.

Figure 13 compares tropical (panel a) and global (panel b) mid-visible AOD and N_{150} evolution from the 3 main simulations **A_Control20**, **B_Control10** and **C_noPinatubo** against the satellite observations from AVHRR. We also compare timeseries of simulated N_{150} at 18 and 22km altitude against the long timeseries OPC measurements from Laramie. Also presented in Figure 13 are results from two additional 10 Tg simulations, designed to test the sensitivity of the model predictions to sub-grid particle formation (run **D_noPrimary10**) and with much reduced new particle formation rate (run **E_ScaledStNuc10**).

Both of these processes are highly uncertain in the stratosphere and the two additional simulations essentially test how robust the model is to changes in the model physics. In the first 12 months after the eruption the tropical and global AOD is around 80% higher in run **A_Control20** than **B_Control10**, but in the second half of 1992 the difference in AOD between the two control runs reduces to only around 10%. In run **D_noPrimary10**, AOD is only very slightly lower than in **B_Control10** suggesting including the source of primary particles has only a minor impact on the aerosol evolution post-Pinatubo. The factor-100 reduced nucleation run **E_ScaledStNuc10** causes a prolonged peak in tropical mid-visible AOD, with values around 10% higher during September 1991, with **E_ScaledStNuc10** continuing to have AOD around 5% higher than **B_Control10** through the remainder of the simulation. Intriguingly, the impact of the nucleation rate reduction on N_{150} is, in the first six months after the eruption, to reduce N_{150} which is opposite to the slight increase in mid-visible AOD. This likely is due to a reduced number of smaller particles growing to larger than 150 nm, with the AOD increase caused by larger particles which will have received more gas to particle transfer of sulphuric acid enhancing condensational growth and increasing their scattering efficiency. In summary however, although these microphysical sensitivities are interesting, the results suggest a low sensitivity to uncertainties in the nucleation rate, and to model treatment of sub-grid particle formation. The low sensitivity gives additional credibility to the aerosol microphysics models, suggesting the models are robust to known uncertainties in some processes in stratospheric conditions.

6 Summary and conclusions

We have extended the UKCA module to incorporate stratospheric sulphur chemistry and updated the process descriptions in the GLOMAP aerosol microphysics module to be applicable for both tropospheric and stratospheric conditions. Using stratospheric aerosol changes after the Mt. Pinatubo as a test case, we have evaluated simulated aerosol properties against a wide range of observations in both quiescent and vol-

canically perturbed conditions. The improvements to the model enable a prognostic treatment of stratospheric aerosol with dynamically varying particle size distribution alongside stratospheric transport and chemistry up to a model top of 80 km.

In general, the model captures the observed distribution and evolution of stratospheric aerosol properties well, in both quiescent and volcanically perturbed conditions. For the Pinatubo test case, the timing of the peak in global aerosol mass and decay timescale are captured well compared to values derived from HIRS satellite measurements (Baran et al., 1993). However, our control simulation of 20 T_g produced much too high a burden of aerosol sulphur, and we find a 10 T_g injection of SO₂ from Pinatubo to be in good agreement with those measurements, and with SAGE-II and AVHRR aerosol optical depth evolution. Modelled extinction in the tropical and NH mid-latitude lower stratosphere shows good agreement with SAGE V7 data in both the mid-visible and near infra-red. However, for the first six months after the eruption simulated AOD and SAD are larger than the satellite measurements, and the model enhancement in R_{eff} is too low (e.g. compared to Bauman et al., 2003). Lack of radiative coupling in these simulations is likely to be the dominant contribution to the high AOD, since radiative heating of the Pinatubo cloud in the tropical lower stratosphere is known to have enhanced upwelling and reduces aerosol optical depth in model simulations (e.g. Young et al., 1994).

To better understand how the particle size distribution was perturbed during the Pinatubo eruption, we have compared against mid-latitude balloon-borne measurements during that time period, allowing a strong observational constraint on concentrations of particles larger than 5, 150, 250, 550, 750 and 1000 nm. Although there have been many model studies covering the Pinatubo period over the 22 yr since the eruption, to our knowledge, this is the first time the full profile of a simulated size distribution in a global model has been compared to these measurements in volcanically perturbed conditions.

In volcanically quiescent conditions, the model finds nucleation only occurs in polar spring, with particles at Laramie in the lower stratosphere originating from the tropical

upper troposphere. In such background conditions the model agrees very well with size distribution observed at Laramie, with only a small proportion of these nucleated particles have grown to 150 nm by coagulation and condensation, with N_5 larger than N_{150} by around a factor of 10. We have investigated the impact on the size distribution of 20 and 10 Tg tropical injections of SO_2 from Pinatubo.

In the first two months after the eruption, nucleation is found to occur throughout the volcanic plume and the large injection of SO_2 leads to strong growth of these particles together with growth of older particles formed in the tropical upper troposphere. Comparing the 10 and 20 Tg control simulations, we find much larger relative difference between concentrations of particles larger than 550 nm between runs **A_Control20** and **B_Control10** than in the smaller particles between 150 and 550 nm, which may be indicative of two types of volcanically enhanced particles. Overall the simulated profile of the particle size distribution agrees remarkably well with the observations, capturing most of the complex shape of the concentration profiles in the different size channels. However, the decay timescale for N_{150} is slower in the model than the observations which leads to an initially modest high bias increasing to around a factor of two by mid 1993 (e.g. Figure 13), with the return to a background size distribution occurring much later in the model. The spatial and temporal evolution of the R_{eff} in the lower stratosphere seen by satellite (Bauman et al., 2003) is also well captured by the model, albeit with a low bias in size compared to the measurements.

Comparing the evolution and altitude of the high biases in extinction to those seen in the OPC profile measurements of the size distribution suggest that the main source of the biases is in particles in the 150 to 550 nm size range in the lowermost stratosphere. The discrepancy could be related to the modal aerosol dynamics failing to capture the differential growth across the particle size range. However, alternative explanation could be too young age-of-air (too rapid STE) could be affecting the simulated stratospheric aerosol evolution. We also note that enhanced upwelling from radiative heating of the enhanced aerosol layer, not included in these uncoupled simulations, will also change the vertical distribution and transport of the aerosol.

Overall, the general good agreement with the size distribution measurements from Laramie and the global effective radius evolution from satellite suggest the modal aerosol microphysics module used in our composition-climate model is capable of representing the variation in particle size distribution in the strongly volcanically perturbed post-Pinatubo period. The sensitivity simulations also suggest that such simulated perturbations to stratospheric aerosol properties are robust to known uncertainties in nucleation rate and sub-grid particle formation. Finally we note that our findings underline the importance of better constraining transport and growth of Aitken-mode-sized particles in the first few months after the eruption to improve prediction of volcanic impacts on climate with stratospheric aerosol microphysics models.

Acknowledgements. We would like to thank P. B. Russell for effective radius data. This work was supported by the UK Natural Environment Research Council (NERC grants NE/E005659/1 and NE/E017150/1). GWM and KSC received funding from the National Centre for Atmospheric Science, one of the NERC research centres. GWM received EU funding from the European Research Council (ERC) under Seventh Framework Programme (FP7) consortium projects MACC and MACC-II (grant agreements 218793 and 283576 respectively). NB, MD, CEJ, FOC were supported as part the UK Integrated Climate Programme funded by the Department for Energy and Climate Change (DECC) and Department for Environment Food and Rural Affairs – DECC/Defra (GA01101). RH was partly funded by German Federal Ministry of Education and Research (BMBF) project ROSA (reference code 01LG1212A) within the ROMIC (Role Of the Middle Atmosphere in Climate) research program. We would also like to thank James Keeble for his help during model development. We acknowledge use of the MONSooN system, a collaborative facility supplied under the Joint Weather and Climate Research Programme, which is a strategic partnership between the UK Met Office and the Natural Environment Research Council. This work has been also supported by NIWA as part of its Government-funded, core research programme. The in situ measurements were supported by the US National Science Foundation. Current measurements are supported under grant number ATM-0437406.

References

- Andres, R. and Kasgnoc, A.: A time-averaged inventory of subaerial volcanic sulfur emissions, *J. Geophys. Res.-Atmos.*, 103, 25 251–25 261, 1998.
- Aquila, V., Oman, L. D., Stolarski, R. S., Colarco, P. R., and Newman, P. A.: Dispersion
5 of the volcanic sulfate cloud from a Mount Pinatubo-like eruption, *Journal of Geophysical Research-Atmospheres*, 117, D06 216, doi:10.1029/2011JD016968, 2012.
- Arfeuille, F., Luo, B. P., Heckendorn, P., Weisenstein, D., Sheng, J. X., Rozanov, E., Schraner, M., Brönnimann, S., Thomason, L. W., and Peter, T.: Uncertainties in modelling the stratospheric warming following Mt. Pinatubo eruption, *Atmos. Chem. Phys. Discuss.*, 13, 4601–
10 4635, 2013.
- Arnold, F., Fabian, R., and Joos, W.: Measurements of the height variation of sulfuric acid vapor concentrations in the stratosphere, *Geophysical Research Letters*, 8, 293–296, 1981.
- Baran, A. J. and Foot, J. S.: New application of the operational sounder HIRS in determining a climatology of sulphuric acid aerosol from the Pinatubo eruption, *J. Geophys. Res.-Atmos.*,
15 99, 25 673–25 679, 1994.
- Baran, A. J., Foot, J. S., and Dibben, P. C.: Satellite detection of volcanic sulfuric-acid aerosol, *Geophysical Research Letters*, 20, 1799–1801, 1993.
- Bauman, J., Russell, P., Geller, M., and Hamill, P.: A stratospheric aerosol climatology from SAGE II and CLAES measurements: 2. Results and comparisons, 1984–1999, *Journal of
20 geophysical research*, 108, D134 383, doi:10.1029/2002JD002993, 2003.
- Bekki, S.: Oxidation of volcanic SO₂: a sink for stratospheric OH and H₂O, *Geophysical Research Letters*, 22, 913–916, 1995.
- Bekki, S. and Pyle, J.: Two dimensional assessment of the impact of aircraft sulphur emissions on the stratospheric sulphate aerosol layer, *J. Geophys. Res.-Atmos.*, 97, 15 839–15 847,
25 1992.
- Bekki, S. and Pyle, J.: A two-dimensional modeling study of the volcanic eruption of Mount Pinatubo, *Journal of Geophysical Research: Atmospheres (1984–2012)*, 99, 18 861–18 869,
1994.
- Bekki, S., Pyle, J. A., Zhong, W., Toumi, R., Haigh, J. D., and Pyle, D. M.: The role of microphysical and chemical processes in prolonging the climate forcing of the Toba eruption, *Geophysical Research Letters*, 23, 2669–2672, 1996.
- Binkowski, F. S. and Roselle, S. J.: Models-3 Community Multiscale Air Quality (CMAQ) model

- aerosol component 1. Model description, *J. Geophys. Res.-Atmos.*, 108, D64 183, doi:10.1029/2001JD001409, 2003.
- Bluth, G. J., Doiron, S. D., Schnetzler, C. C., Krueger, A. J., and Walter, L. S.: Global tracking of the SO₂ clouds from the June, 1991 Mount Pinatubo eruptions, *Geophysical Research Letters*, 19, 151–154, 1992.
- Bluth, G. J. S., Rose, W. I., Sprod, I. E., and Krueger, A. J.: Stratospheric loading of sulfur from explosive volcanic eruptions, *Journal of Geology*, 105, 671–683, 1997.
- Braesicke, P., Keeble, J., Yang, X., Stiller, G., Kellmann, S., Abraham, N. L., Archibald, A., Telford, P., and Pyle, J. A.: Circulation anomalies in the Southern Hemisphere and ozone changes, *Atmos. Chem. Phys.*, 13, 10677–10688, 2013.
- Brühl, C., Lelieveld, J., Höpfner, M., and Tost, H.: Stratospheric SO₂ and sulphate aerosol, model simulations and satellite observations, *Atmospheric Chemistry and Physics Discussions*, 13, 11395–11425, doi:10.5194/acpd-13-11395-2013, 2013.
- Campbell, P. and Deshler, T.: Condensation nuclei measurements in the midlatitude (1982–2012) and Antarctic (1986–2010) stratosphere between 20 and 35 km, *Journal of Geophysical Research: Atmospheres*, 119, 137–152, 2014.
- Carslaw, K. and Kärcher, B.: Stratospheric aerosol processes. In: Thomason L. and Peter Th. (Eds.) SPARC Assessment of Stratospheric Aerosol Properties (ASAP), pp. 1–28, SPARC Report No. 4, World Climate Research Programme, 2006.
- Carslaw, K. S., Luo, B., and Peter, T.: An analytic expression for the composition of aqueous HNO₃–H₂SO₄ stratospheric aerosols including gas phase removal of HNO₃, *Geophysical Research Letters*, 22, 1877–1880, 1995.
- Carver, G. D., Brown, P. D., and Wild, O.: The ASAD atmospheric chemistry integration package and chemical reaction database, *Computer Physics Communications*, 105, 197–215, 1997.
- Chipperfield, M.: New version of the TOMCAT/SLIMCAT offline chemical transport model: Intercomparison of stratospheric tracer experiments, *Quarterly Journal of the Royal Meteorological Society*, 132, 1179–1203, 2006.
- Chipperfield, M. and Pyle, J.: Model sensitivity studies of Arctic ozone depletion, *J. Geophys. Res.-Atmos.*, 103, 28389–28403, 1998.
- Chipperfield, M., Liang, Q., Strahan, S., Morgenstern, O., Dhomse, S., Abraham, N., Archibald, A., Bekki, S., Braesicke, P., Di Genova, G., Fleming, E. L., Hardiman, S. C., Iachetti, D., Jackman, C. H., Kinnison, D. E., Marchand, M., Pitari, G., Pyle, J. A., Rozanov, E., Stenke, A., and Tummon, F.: Multimodel estimates of atmospheric lifetimes of long-lived ozone-

- depleting substances: Present and future, *Journal of Geophysical Research: Atmospheres*, 119, 2555–2573, 2014.
- D’Almeida, G. A., Koepke, P., and Shettle, E. P.: Atmospheric aerosols: global climatology and radiative characteristics, A. Deepak Pub. Hampton, Virginia, USA, 1991.
- 5 Damadeo, R., Zawodny, J., Thomason, L., and Iyer, N.: SAGE version 7.0 algorithm: application to SAGE II, *Atmospheric Measurement Techniques Discussions*, 6, 5101–5171, 2013.
- Dee, D. P., Uppala, S. M., Simmons, A. J., Berrisford, P., Poli, P., Kobayashi, S., Andrae, U.,
Balmaseda, M. A., Balsamo, G., Bauer, P., Bechtold, P., Beljaars, A. C. M., van de Berg, L.,
Bidlot, J., Bormann, N., Delsol, C., Dragani, R., Fuentes, M., Geer, A. J., Haimberger, L.,
10 Healy, S., Hersbach, H., Holm, E. V., Isaksen, L., Kallberg, P., Koehler, M., Matricardi, M.,
McNally, A. P., Monge-Sanz, B. M., Morcrette, J.-J., Peubey, C., de Rosnay, P., Tavolato, C.,
Thapaut, J.-N., and Vitart, F.: The ERA-Interim reanalysis: Configuration and performance
of the data assimilation system, *Quart. J. Roy. Meteorol. Soc.*, 133, 1972–1990, 2011.
- Deshler, T.: In situ measurements of Pinatubo aerosol over Kiruna on four days between 18
15 January and 13 February 1992, *Geophysical research letters*, 21, 1323–1326, 1994.
- Deshler, T.: A review of global stratospheric aerosol: Measurements, importance, life cycle,
and local stratospheric aerosol, *Atmospheric Research*, 90, 223–232, 2008.
- Deshler, T., Hofmann, D., Johnson, B., and Rozier, W.: Balloonborne measurements of the
Pinatubo aerosol size distribution and volatility at Laramie, Wyoming during the summer of
20 1991, *Geophysical Research Letters*, 19, 199–202, 1992.
- Deshler, T., Johnson, B. J., and Rozier, W. R.: Balloonborne measurements of Pinatubo aerosol
during 1991 and 1992 at 41 °N: Vertical profiles, size distribution, and volatility, *Geophysical
Research Letters*, 20, 1435–1438, doi:10.1029/93GL01337, 1993.
- Deshler, T., Hervig, M. E., Hofmann, D. J., Rosen, J. M., and Liley, J. B.: Thirty years of in situ
25 stratospheric aerosol size distribution measurements from Laramie, Wyoming (41 degrees
N), using balloon-borne instruments, *Journal of Geophysical Research-Atmospheres*, 108,
D54 167, doi:10.1029/2002JD002514, 2003.
- Dhomse, S., Weber, M., Wohltmann, I., Rex, M., and Burrows, J. P.: On the possible causes
of recent increases in northern hemispheric total ozone from a statistical analysis of satellite
30 data from 1979 to 2003, *Atmospheric Chemistry and Physics*, 6, 1165–1180, 2006.
- Driscoll, S., Bozzo, A., Gray, L. J., Robock, A., and Stenchikov, G.: Coupled Model Intercom-
parison Project 5 (CMIP5) simulations of climate following volcanic eruptions, *J. Geophys.
Res.-Atmos.*, 117, D17 105, doi:10.1029/2012JD017607, 2012.

English, J. M., Toon, O. B., and Mills, M. J.: Microphysical simulations of sulfur burdens from stratospheric sulfur geoengineering, *Atmospheric Chemistry and Physics*, 12, 4775–4793, 2012.

English, J. M., Toon, O. B., and Mills, M. J.: Microphysical simulations of large volcanic eruptions: Pinatubo and Toba, *J. Geophys. Res.-Atmos.*, 118, 1880–1895, doi:10.1002/jgrd.50196, 2013.

Graf, H. F., Kirchner, I., Robock, A., and Schult, I.: Pinatubo eruption winter climate effects: Model versus observations, *Climate Dynamics*, 9, 81–93, 1993.

Grainger, R., Lambert, A., Taylor, F., Remedios, J., Rodgers, C., Corney, M., and Kerridge, B.: Infrared absorption by volcanic stratospheric aerosols observed by ISAMS, *Geophysical research letters*, 20, 1283–1286, 1993.

Guo, S., Bluth, G. J., Rose, W. I., Watson, I. M., and Prata, A.: Re-evaluation of SO₂ release of the 15 June 1991 Pinatubo eruption using ultraviolet and infrared satellite sensors, *Geochemistry, Geophysics, Geosystems*, 5, Q04 001, doi:10.1029/2003GC000654, 2004a.

Guo, S., Rose, W. I., Bluth, G. J., and Watson, I. M.: Particles in the great Pinatubo volcanic cloud of June 1991: The role of ice, *Geochemistry, Geophysics, Geosystems*, 5, 2004b.

Hall, T. M., Waugh, D. W., Boering, K. A., and Plumb, R. A.: Evaluation of transport in stratospheric models, *J. Geophys. Res.-Atmos.*, 104, 18815–18839, 1999.

Hamill, P., Jensen, E. J., Russell, P., and Bauman, J. J.: The life cycle of stratospheric aerosol particles, *Bulletin of the American Meteorological Society*, 78, 1395–1410, 1997.

Hamill, P., Brogniez, C., Thomason, L., Deshler, T., Antuña, J., Baumgardner, D., Bevilacqua, R., Brock, C., David, C., Fussen, D., Hervig, M., Hostettler, C. A., Lee, S.-H., Mergenthaler, J., Osborn, M. T., Raga, G., Reeves, J. M., Rosen, J., and Wilson, J. C.: Instrument Descriptions. In: Thomason L. and Peter Th. (Eds.) SPARC Assessment of Stratospheric Aerosol Properties (ASAP), pp. 77–106, SPARC Report No. 4, World Climate Research Programme, 2006.

Hansen, J., Lacis, A., Ruedy, R., and Sato, M.: Potential climate impact of Mount Pinatubo eruption, *Geophysical Research Letters*, 19, 215–218, 1992.

Hewitt, H. T., Copsey, D., Culverwell, I. D., Harris, C. M., Hill, R. S. R., Keen, A. B., McLaren, A. J., and Hunke, E. C.: Design and implementation of the infrastructure of HadGEM3: the next-generation Met Office climate modelling system, *Geoscientific Model Development*, 4, 223–253, 2011.

Hofmann, D. and Rosen, J.: Balloonborne observations of stratospheric aerosol and conden-

- sation nuclei during the year following the Mt. St. Helens eruption, *Journal of Geophysical Research: Oceans*, 87, 11 039–11 061, 1982.
- Holton, J. R. and Tan, H.-C.: The influence of the equatorial quasi-biennial oscillation on the global circulation at 50 mb, *Journal of the Atmospheric Sciences*, 37, 2200–2208, 1980.
- 5 Holton, J. R., Haynes, P. H., McIntyre, M. E., Douglass, A. R., Rood, R. B., and Pfister, L.: Stratosphere-troposphere exchange, *Reviews of Geophysics*, 33, 403–439, 1995.
- Hommel, R., Timmreck, C., and Graf, H.: The global middle-atmosphere aerosol model MAECHAM5-SAM2: comparison with satellite and in-situ observations, *Geoscientific Model Development*, 4, 809–834, 2011.
- 10 Hurrell, J. W., Hack, J. J., Shea, D., Caron, J. M., and Rosinski, J.: A new sea surface temperature and sea ice boundary dataset for the Community Atmosphere Model, *Journal of Climate*, 21, 5145–5153, 2008.
- Jäger, H.: The Pinatubo eruption cloud observed by lidar at Garmisch-Partenkirchen, *Geophysical research letters*, 19, 191–194, 1992.
- 15 Jones, C., Hughes, J., Bellouin, N., Hardiman, S., Jones, G., Knight, J., Liddicoat, S., O'Connor, F., Andres, R. J., and Bell, C.: The HadGEM2-ES implementation of CMIP5 centennial simulations, *Geoscientific Model Development*, 4, 543–570, 2011.
- Kerminen, V.-M. and Kulmala, M.: Analytical formulae connecting the "real" and the "apparent" nucleation rate and the nuclei number concentration for atmospheric nucleation events, *Journal of Aerosol Science*, 33, 609–622, 2002.
- 20 Kettle, A. and Andreae, M.: Flux of dimethylsulfide from the oceans: A comparison of updated data sets and flux models, *J. Geophys. Res.-Atmos.*, 105, 26 793–26 808, 2000.
- Kokkola, H., Hommel, R., Kazil, J., Niemeier, U., Partanen, A.-I., Feichter, J., and Timmreck, C.: Aerosol microphysics modules in the framework of the ECHAM5 climate model – inter-comparison under stratospheric conditions, *Geoscientific Model Development*, 2, 97–112, doi:10.5194/gmd-2-97-2009, 2009.
- 25 Kreidenweis, S. M., Walcek, C. J., Feingold, G., Gong, W., Jacobson, M. Z., Kim, C.-H., Liu, X., Penner, J. E., Nenes, A., and Seinfeld, J. H.: Modification of aerosol mass and size distribution due to aqueous-phase SO₂ oxidation in clouds: Comparisons of several models, *Journal of geophysical research*, 108, D74 213, doi:10.1029/2002JD002697, 2003.
- 30 Kulmala, M. and Laaksonen, A.: Binary nucleation of water-sulfuric acid system: Comparison of classical theories with different H₂SO₄ saturation vapor pressures, *The Journal of Chemical Physics*, 93, 696, 1990.

- Kulmala, M., Laaksonen, A., and Pirjola, L.: Parameterizations for sulfuric acid/water nucleation rates, *J. Geophys. Res.-Atmos.*, 103, 8301–8307, 1998.
- Labitzke, K. and McCormick, M.: Stratospheric temperature increases due to Pinatubo aerosols, *Geophysical Research Letters*, 19, 207–210, 1992.
- 5 Lacis, A., Hansen, J., and Sato, M.: Climate forcing by stratospheric aerosols, *Geophysical Research Letters*, 19, 1607–1610, 1992.
- Lamarque, J.-F., Bond, T. C., Eyring, V., Granier, C., Heil, A., Klimont, Z., Lee, D., Liousse, C., Mieville, A., and Owen, B.: Historical (1850–2000) gridded anthropogenic and biomass burning emissions of reactive gases and aerosols: methodology and application, *Atmospheric Chemistry and Physics*, 10, 7017–7039, 2010.
- 10 Lambert, A., Grainger, R., Remedios, J., Rodgers, C., Corney, M., and Taylor, F.: Measurements of the evolution of the Mt. Pinatubo aerosol cloud by ISAMS, *Geophysical research letters*, 20, 1287–1290, 1993.
- Liss, P. S. and Merlivat, L.: Air-sea gas exchange rates: Introduction and synthesis, pp. 113–127, Springer, Netherlands, 1986.
- 15 Long, C. S. and Stowe, L. L.: USING THE NOAA AVHRR TO STUDY STRATOSPHERIC AEROSOL OPTICAL THICKNESSES FOLLOWING THE MT-PINATUBO ERUPTION, *Geophysical Research Letters*, 21, 2215–2218, 1994.
- Mann, G., Carslaw, K., Spracklen, D., Ridley, D., Manktelow, P., Chipperfield, M., Pickering, S., and Johnson, C.: Description and evaluation of GLOMAP-mode: a modal global aerosol microphysics model for the UKCA composition-climate model, *Geoscientific Model Development*, 3, 519–551, 2010.
- 20 Mann, G., Carslaw, K., Ridley, D., Spracklen, D., Pringle, K., Merikanto, J., Korhonen, H., Schwarz, J., Lee, L., Manktelow, P., Woodhouse, M., Schmidt, A., Breider, T., Emmerson, K., Reddington, C., Chipperfield, M., and Pickering, S.: Intercomparison of modal and sectional aerosol microphysics representations within the same 3-D global chemical transport model, *Atmospheric Chemistry and Physics*, 12, 4449–4476, 2012.
- 25 Martin, E., George, C., and Mirabel, P.: Densities and surface tensions of H₂SO₄/HNO₃/H₂O solutions, *Geophysical Research Letters*, 27, 197–200, 2000.
- 30 McCormick, M. and Veiga, R.: SAGE II measurements of early Pinatubo aerosols, *Geophysical Research Letters*, 19, 155–158, 1992.
- McCormick, M. P., Thomason, L. W., and Trepte, C. R.: Atmospheric effects of the Mt Pinatubo eruption, *Nature*, 373, 399–404, 1995.

- Mills, M. J., Toon, O. B., Vaida, V., Hintze, P. E., Kjaergaard, H. G., Schofield, D. P., and Robinson, T. W.: Photolysis of sulfuric acid vapor by visible light as a source of the polar stratospheric CN layer, *J. Geophys. Res.-Atmos.*, 110, D08 201, doi:10.1029/2004JD005519D8, 2005.
- 5 Morgenstern, O., Braesicke, P., O'Connor, F., Bushell, A., Johnson, C., Osprey, S., and Pyle, J.: Evaluation of the new UKCA climate-composition model Part 1: The stratosphere, *Geoscientific Model Development*, 2, 43–57, 2009.
- Neu, J. L., Prather, M. J., and Penner, J. E.: Global atmospheric chemistry: Integrating over fractional cloud cover, *J. Geophys. Res.-Atmos.*, 112, D11 306, doi:10.1029/2006JD008007, 10 2007.
- Niemeier, U., Timmreck, C., Graf, H.-F., Kinne, S., Rast, S., and Self, S.: Initial fate of fine ash and sulfur from large volcanic eruptions, *Atmospheric Chemistry and Physics*, 9, 9043–9057, 2009.
- Oman, L., Robock, A., Stenchikov, G. L., Thordarson, T., Koch, D., Shindell, D. T., and Gao, C. C.: Modeling the distribution of the volcanic aerosol cloud from the 1783-1784 Laki eruption, *Journal of Geophysical Research-Atmospheres*, 111, D12 209, doi:10.1029/15 2005JD006899, 2006.
- Pitari, G. and Mancini, E.: Short-term climatic impact of the 1991 volcanic eruption of Mt. Pinatubo and effects on atmospheric tracers, *Natural Hazards and Earth System Science*, 2, 20 91–108, doi:10.5194/nhess-2-91-2002, 2002.
- Reeves, J., Wilson, J., Brock, C., and Bui, T.: Comparison of aerosol extinction coefficients, surface area density, and volume density from SAGE II and in situ aircraft measurements, *J. Geophys. Res.-Atmos.*, 113, D10 202, doi:10.1029/2007JD009357113, 2008.
- Robock, A.: Volcanic eruptions and climate, *Reviews of Geophysics*, 38, 191–219, 2000.
- 25 Robock, A. and Mao, J.: Winter warming from large volcanic eruptions, *Geophysical Research Letters*, 19, 2405–2408, 1992.
- Rosen, J. M.: The vertical distribution of dust to 30 kilometers, *Journal of Geophysical Research*, 69, 4673–4676, 1964.
- Russell, P., Livingston, J., Pueschel, R., Bauman, J., Pollack, J., Brooks, S., Hamill, P., Thomason, L., Stowe, L., and Deshler, T.: Global to microscale evolution of the Pinatubo volcanic aerosol derived from diverse measurements and analyses, *Journal of geophysical research*, 30 101, 18 745–18,763, 1996.
- Sander, S., Friedl, R., Golden, D., Kurylo, M., Huie, R., Orkin, V., Moortgat, G., Wine, P., Ravis-

- hankara, A., Kolb, C., Molina, M., Finlayson-Pitts, B., Huie, R., Orkin, V. L., and Keller-Rudek, H.: Chemical kinetics and photochemical data for use in atmospheric studies, NASA Panel for Data Evaluation, Evaluation number 15, JPL Publication 06-2, vol. 4915, Jet Propulsion Laboratory, California Institute of Technology, Pasadena, California, 2006.
- 5 Sato, M., Hansen, J. E., McCormick, M. P., and Pollack, J. B.: Stratospheric aerosol optical depths, 1850–1990, *J. Geophys. Res.-Atmos.*, 98, 22 987–22 994, 1993.
- Saunders, R. W., Dhomse, S., Tian, W. S., Chipperfield, M. P., and Plane, J. M. C.: Interactions of meteoric smoke particles with sulphuric acid in the Earth’s stratosphere, *Atmospheric Chemistry and Physics*, 12, 4387–4398, 2012.
- 10 Scaife, A. A., Spanghel, T., Fereday, D. R., Cubasch, U., Langematz, U., Akiyoshi, H., Bekki, S., Braesicke, P., Butchart, N., and Chipperfield, M. P.: Climate change projections and stratosphere-troposphere interaction, *Climate Dynamics*, 38, 2089–2097, 2012.
- Solomon, S., Portmann, R. W., Garcia, R. R., Thomason, L. W., Poole, L. R., and McCormick, M. P.: The role of aerosol variations in anthropogenic ozone depletion at northern midlatitudes, *Journal of Geophysical Research-Atmospheres*, 101, 6713–6727, 1996.
- 15 Solomon, S., Daniel, J., Neely, R., Vernier, J.-P., Dutton, E., and Thomason, L.: The persistently variable “background” stratospheric aerosol layer and global climate change, *Science*, 333, 866–870, 2011.
- SPARC: SPARC Assessment of stratospheric aerosol properties (ASAP) SPARC Report No. 4, World Climate Research Programme, WCRP-124,WMO/TD-No.1295, 2006.
- 20 SPARC: SPARC Report on the Evaluation of Chemistry-Climate Models, World Climate Research Programme, WCRP-132,WMO/TD-No.1526, 2010.
- SPARC: Lifetime of halogen source gases WMO Ozone Research and Monitoring Project Report No. 6, World Climate Research Programme, WCRP-113,WMO/TD-No.XXXX, 2013.
- 25 Spracklen, D. V., Pringle, K. J., Carslaw, K. S., Chipperfield, M. P., and Mann, G. W.: A global off-line model of size-resolved aerosol microphysics: I. Model development and prediction of aerosol properties, *Atmospheric Chemistry and Physics*, 5, 2227–2252, doi: 10.5194/acp-5-2227-2005, 2005.
- Stenchikov, G. L., Kirchner, I., Robock, A., Graf, H., Antuna, J. C., Grainger, R., Lambert, A., and Thomason, L.: Radiative forcing from the 1991 Mount Pinatubo volcanic eruption, *J. Geophys. Res.-Atmos.*, 103, 13 837–13 857, 1998.
- 30 Stier, P., Feichter, J., Kinne, S., Kloster, S., Vignati, E., Wilson, J., Ganzeveld, L., Tegen, I., Werner, M., and Balkanski, Y.: The aerosol-climate model ECHAM5-HAM, *Atmospheric*

Chemistry and Physics, 5, 1125–1156, 2005.

Stokes, R. and Robinson, R.: Interactions in aqueous nonelectrolyte solutions. I. Solute-solvent equilibria, *The Journal of Physical Chemistry*, 70, 2126–2131, 1966.

5 Strahan, S. E., Douglass, A. R., Stolarski, R. S., Akiyoshi, H., Bekki, S., Braesicke, P., Butchart, N., Chipperfield, M. P., Cugnet, D., Dhomse, S., Frith, S. M., Gettelman, A., Hardiman, S. C., Kinnison, D. E., Lamarque, J. F., Mancini, E., Marchand, M., Michou, M., Morgenstern, O., Nakamura, T., Olivie, D., Pawson, S., Pitari, G., Plummer, D. A., Pyle, J. A., Scinocca, J. F., Shepherd, T. G., Shibata, K., Smale, D., Teysse, H., Tian, W., and Yamashita, Y.: Using transport diagnostics to understand chemistry climate model ozone simulations, *Journal of Geophysical Research-Atmospheres*, 116, D17 302, doi:doi:10.1029/2010JD015360, 2011.

10 Taylor, K. E., Stouffer, R. J., and Meehl, G. A.: An overview of CMIP5 and the experiment design, *Bulletin of the American Meteorological Society*, 93, 485–498, 2012.

Telford, P., Abraham, N., Archibald, A., Braesicke, P., Dalvi, M., Morgenstern, O., O'Connor, F., Richards, N., and Pyle, J.: Implementation of the Fast-JX Photolysis scheme (v6. 4) into the UKCA component of the MetUM chemistry-climate model (v7. 3), *Geoscientific Model Development*, 6, 161–177, 2013.

Textor, C., Schulz, M., Guibert, S., Kinne, S., Balkanski, Y., Bauer, S., Berntsen, T., Berglen, T., Boucher, O., Chin, M., et al.: Analysis and quantification of the diversities of aerosol life cycles within AeroCom, *Atmospheric Chemistry and Physics*, 6, 1777–1813, 2006.

20 Thomason, L., Poole, L., and Deshler, T.: A global climatology of stratospheric aerosol surface area density deduced from Stratospheric Aerosol and Gas Experiment II measurements 1984–1994, *J. Geophys. Res.-Atmos.*, 102, 8967–8976, 1997.

Timmreck, C.: Three-dimensional simulation of stratospheric background aerosol: First results of a multiannual general circulation model simulation, *Journal of Geophysical Research-Atmospheres*, 106, 28 313–28 332, 2001.

25 Timmreck, C., Graf, H.-F., and Feichter, J.: Simulation of Mt. Pinatubo volcanic aerosol with the Hamburg climate model ECHAM4, *Theoretical and Applied Climatology*, 62, 85–108, 1999.

Toohey, M., Krüger, K., Niemeier, U., and Timmreck, C.: The influence of eruption season on the global aerosol evolution and radiative impact of tropical volcanic eruptions, *Atmospheric Chemistry and Physics*, 11, 12 351–12 367, 2011.

30 Trepte, C. R. and Hitchman, M. H.: Tropical stratospheric circulation deduced from satellite aerosol data, *Nature*, 355, 626–628, 1992.

Vehkamäki, H., Kulmala, M., Napari, I., Lehtinen, K. E., Timmreck, C., Noppel, M., and Laak-

- sonen, A.: An improved parameterization for sulfuric acid–water nucleation rates for tropospheric and stratospheric conditions, *Journal of Geophysical Research*, 107, D224 622, doi:10.1029/2002JD002184, 2002.
- 5 Vignati, E., Wilson, J., and Stier, P.: M7: An efficient size Resolved aerosol microphysics module for large scale aerosol transport models, *J. Geophys. Res.-Atmos.*, 109, D22 202, doi:10.1029/2003JD004485, 2004.
- Weber, M., Dhomse, S., Wittrock, F., Richter, A., Sinnhuber, B. M., and Burrows, J. P.: Dynamical control of NH and SH winter/spring total ozone from GOME observations in 1995-2002, *Geophysical Research Letters*, 30, 2003.
- 10 Weisenstein, D., Bekki, S., Mills, M., Pitari, G., and Timmreck, C.: Modeling of stratospheric aerosols. In: Thomason L. and Peter Th. (Eds.) SPARC Assessment of Stratospheric Aerosol Properties (ASAP), pp. 219–272, SPARC Report No. 4, World Climate Research Programme, 2006.
- Weisenstein, D. K., Yue, G. K., Ko, M. K. W., Sze, N. D., Rodriguez, J. M., and Scott, C. J.: 15 A two-dimensional model of sulfur species and aerosols, *Journal of Geophysical Research-Atmospheres*, 102, 13 019–13 035, 1997.
- Wild, O., Zhu, X., and Prather, M. J.: Fast-J: Accurate simulation of in-and below-cloud photolysis in tropospheric chemical models, *Journal of Atmospheric Chemistry*, 37, 245–282, 2000.
- 20 Wilson, J., Cuvelier, C., and Raes, F.: A modeling study of global mixed aerosol fields, *J. Geophys. Res.-Atmos.*, 106, 34 081–34 108, 2001.
- WMO: Scientific Assessment of Ozone Depletion: 2010, Global Ozone Research and Monitoring Project Report 52, World Meteorological Organization, Geneva, 2011.
- Young, R. E., Houben, H., and Toon, O. B.: Radiatively forced dispersion of the Mt. Pinatubo 25 volcanic cloud and induced temperature perturbations in the stratosphere during the first few months following the eruption, *Geophysical Research Letters*, 21, 369–372, 1994.
- Zdanovskii, A.: New methods for calculating solubilities of electrolytes in multicomponent systems, *Zh. Fiz. Khim*, 22, 1475–1485, 1948.

Table 1. Additional sulphur chemistry reactions and rates within UKCA, W = Weisenstein et al. (1997), JPL = Sander et al. (2006), K03 = Kreidenweis et al. (2003)

	Rate	Reference
DMS + O(³ P) → SO ₂	$1.3 \times 10^{-11} \exp(410/T)$	W, JPL
DMS + OH → SO ₂	$1.2 \times 10^{-11} \exp(-260/T)$	W
DMS + OH → MSA + SO ₂	$3.04 \times 10^{-12} \exp(350/T) \cdot (\gamma/1 + \gamma)$ $\gamma = 5.53 \times 10^{-31} \exp(7460/T) \times [\text{O}_2]$	W
DMS + NO ₃ → SO ₂	$1.9 \times 10^{-13} \exp(500/T)$	W
OCS + O(³ P) → CO + SO ₂	$2.1 \times 10^{-11} \exp(-2200/T)$	W, JPL
OCS + OH → CO ₂ + SO ₂	$1.1 \times 10^{-13} \exp(-1200/T)$	W, JPL
SO ₂ + OH + M → SO ₃ + HO ₂	$k(T) = \frac{A}{1+B} \times 0.6^{(1+(\log B)^2)^{-1}}$ $A = 3.0 \times 10^{-31} \times (300/T)^{3.3}$ $B = A/1.5 \times 10^{-12}$	W
SO ₂ + O ₃ → SO ₃	$3.0 \times 10^{-12} \exp(-7000/T)$	W, JPL
SO ₃ + H ₂ O → H ₂ SO ₄	$8.5 \times 10^{-41} \exp(6540/T) \cdot [\text{H}_2\text{O}]$	JPL
SO ₂ + H ₂ O ₂ ^{aqueous} → SO ₄		K03
OCS + hν → CO + SO ₂	Photolysis	W
H ₂ SO ₄ + hν → SO ₃ + OH	Photolysis	W
SO ₃ + hν → SO ₂ + O(³ P)	Photolysis	W

Table 2. Microphysical parameter settings used in model simulations.

Run	SO ₂ Injection	Nucleation	Primary S Emission
A_Control20	20 Tg (19–27 km)	Standard	Yes
B_Control10	10 Tg (19–27 km)	Standard	Yes
C_noPinatubo	No	Standard	Yes
D_noPrimary10	10 Tg (19–27 km)	Standard	No
E_ScaledStNuc10	10 Tg (19–27 km)	×0.01 in stratosphere	Yes

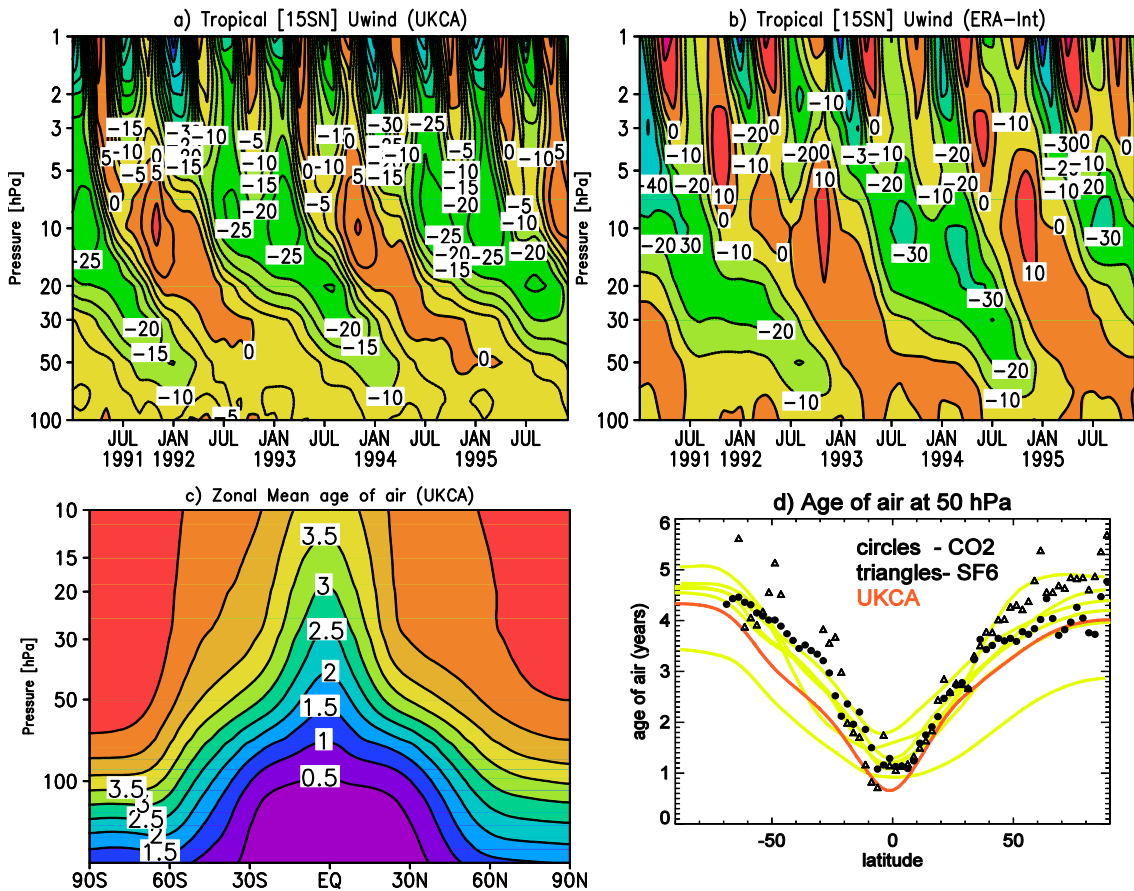


Fig. 1. (a) Model simulated tropical (15° S–15° N) mean monthly mean zonal wind (ms⁻¹, QBO propagation). (b) Same as (a) but from ERA-interim reanalysis data (Dee et al., 2011). (c) Zonal mean age-of-air (years, mean 1991–2000), and (d) mean age of air (1991–2000) comparison at 50 hPa. Triangles and filled circles show estimated age-of-air from CO₂ and SF₆ (Hall et al., 1999). Mean age-of-air from various CCMs which participated in SPARC Lifetime Assessment are shown with yellow lines and one from this study is shown with the red line.

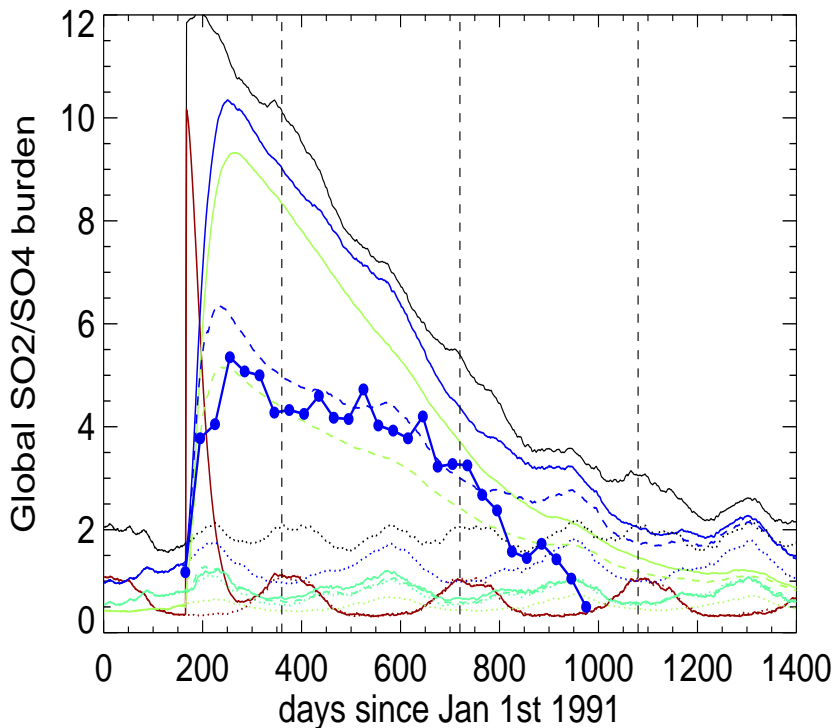


Fig. 2. Time series of the global burden (in Tg of sulphur) of SO_2 (red), total sulphur (includes both SO_2 and aerosol, black), aerosol sulphur (dark blue) for runs **A_Control20** (solid lines), **B_Control10** (dashed lines), and **C_noPinatubo** (dotted lines). Integrated aerosol sulphur burdens in the UTS and lower-middle troposphere (determined by above or below 400 hPa) are also shown with green and aqua lines, respectively. The aerosol burden derived by Baran and Foot (1994) using HIRS measurements is shown by the blue line with filled circles.

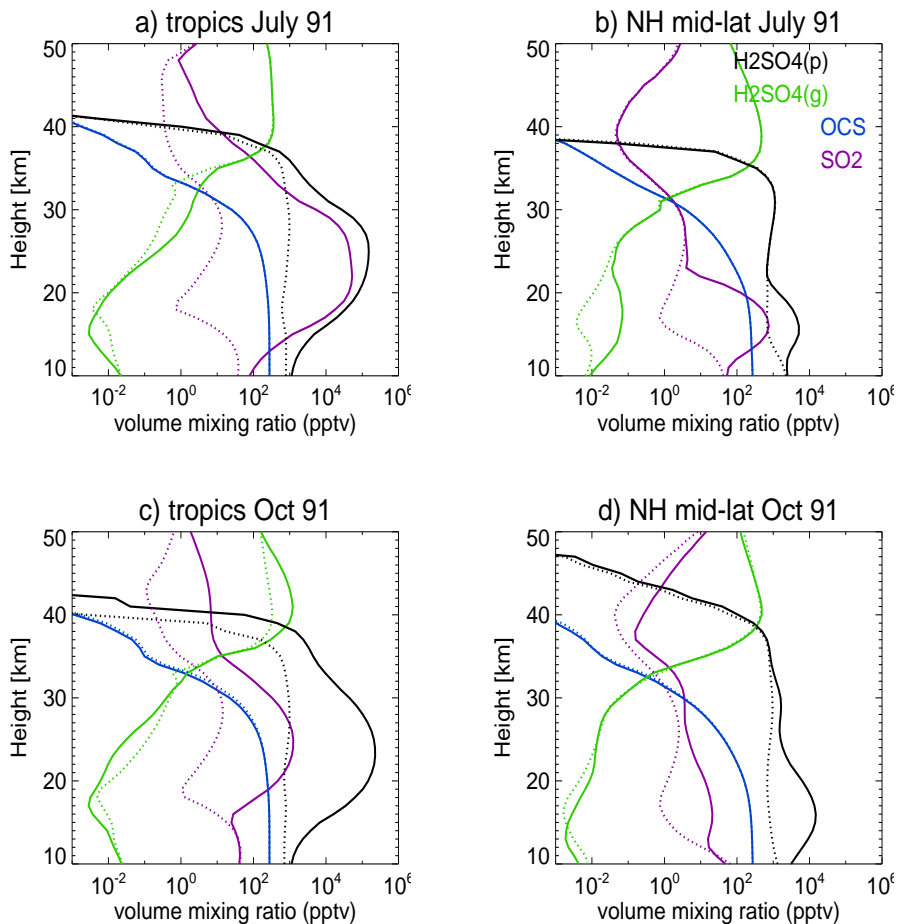


Fig. 3. Volume mixing ratios of various sulphur containing species (pptv) in the tropics (20° S– 20° N, left) and NH mid-latitudes (35 – 60° N, right) during July 1991 (top) and October 1991 (bottom). Gas-phase and particle phase H₂SO₄ ratios are shown with black and green lines, respectively. OCS and SO₂ are shown with blue and magenta lines, respectively. Mixing ratios from runs **A_Control20** and **C_noPinatubo** are shown with solid and dashed lines, respectively.

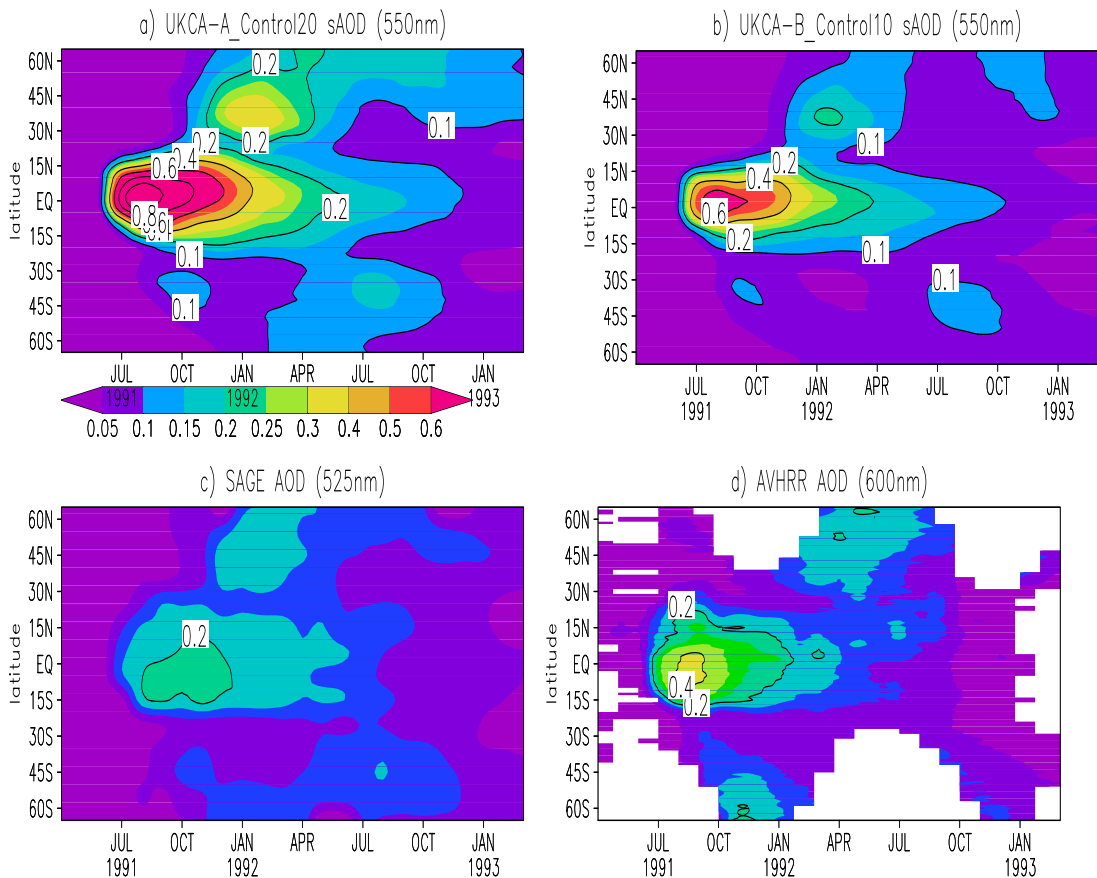


Fig. 4. Time series of model simulated zonal mean stratosphere-only (integrated from the tropopause to top of the atmosphere) AOD derived using 525 nm extinctions for runs **(a) A_Control20** and **(b) B_Control10**. **(c)** and **(d)** show the stratospheric AOD derived using SAGE II (525 nm) and AVHRR (600 nm) measurements. AVHRR AOD shown in **(d)** are after removal of background tropospheric AOD from 522 months before the eruption, see Long and Stowe 1994).

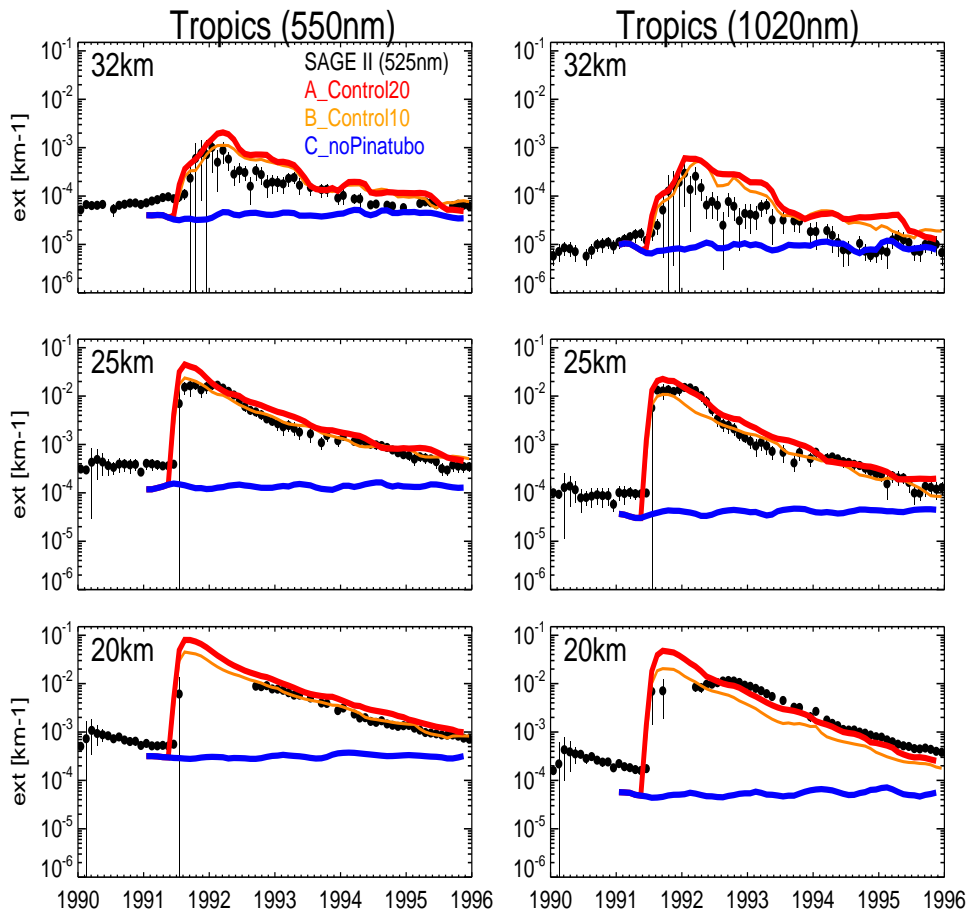


Fig. 5. Comparison between modelled and SAGE II (V7.0) retrieved extinction at 525 nm (left) and 1020 nm (right) in the tropics (20° S–20° N) for 20 km (bottom), 25 km (middle) and 32 km (top). Extinctions from runs **A_Control20**, **B_Control10** and **C_noPinatubo** are shown with red, orange and blue lines, respectively. Standard deviation ($1-\sigma$) derived using all SAGE II measurements used to calculate monthly mean values are shown with vertical black lines.

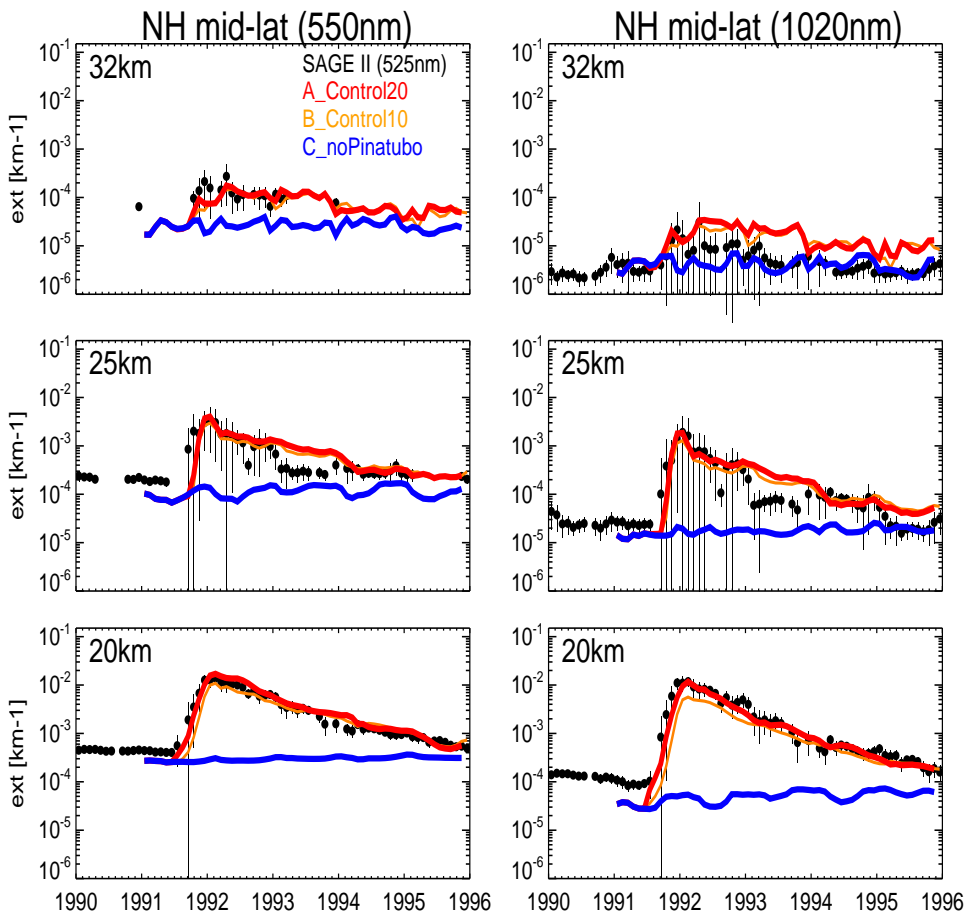


Fig. 6. Same as Fig. 5 but for NH mid-latitudes ($35\text{--}65^\circ\text{ N}$).

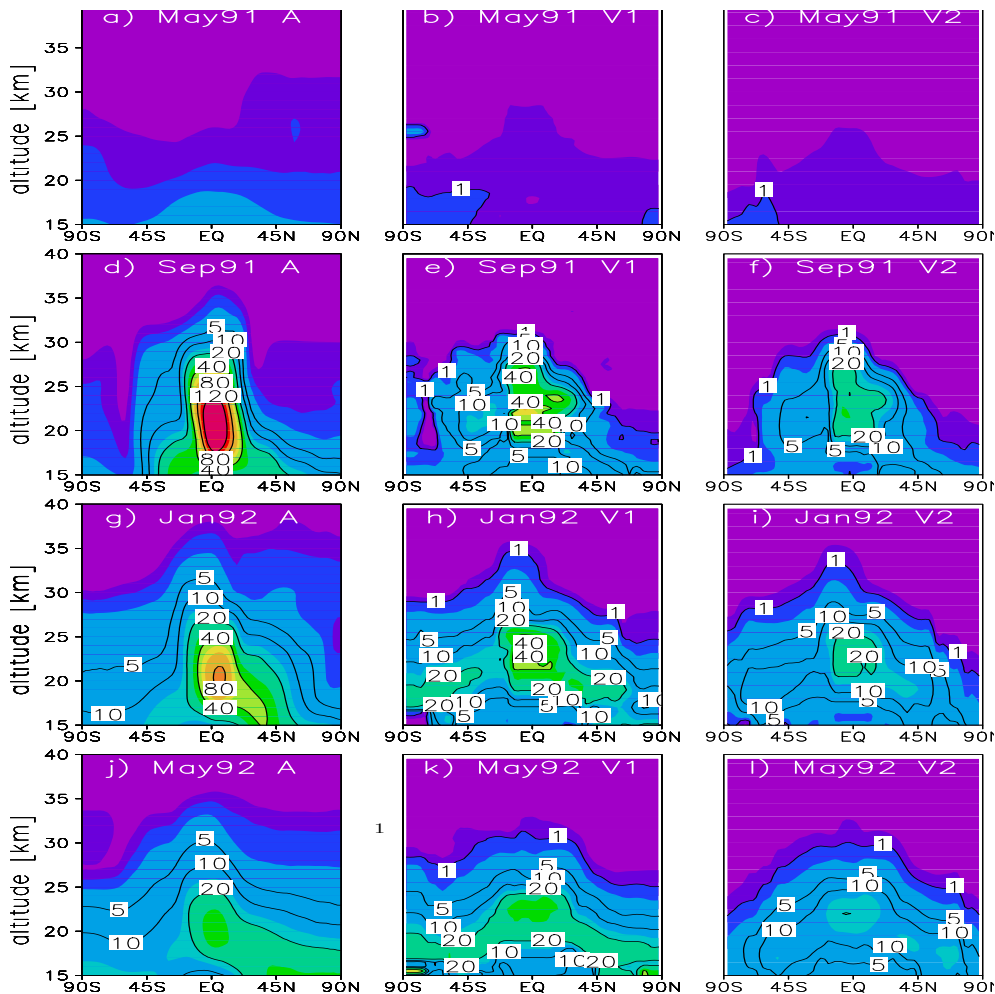


Fig. 7. Comparison between zonal mean modelled (run **A_Control20**) and satellite-derived V1 and V2 SAD ($\mu\text{m}^2\text{cm}^{-3}$) from SPARC (2006) and Arfeuille et al. (2013), respectively, for various months before and after the eruption.

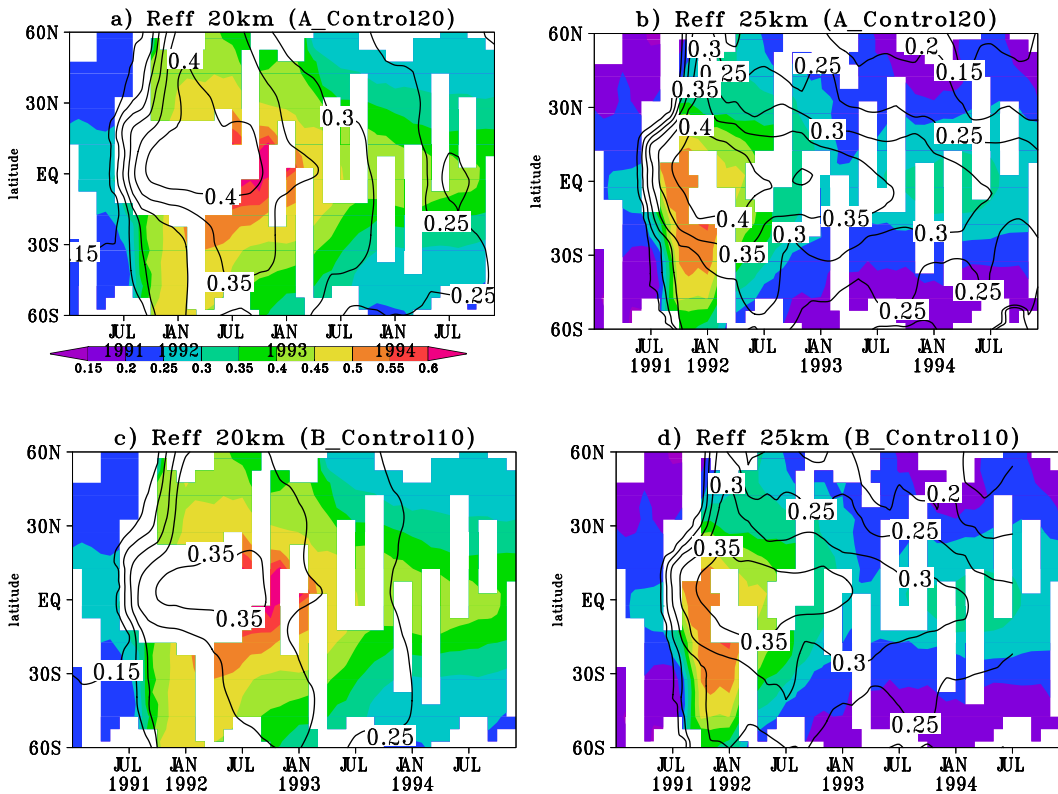


Fig. 8. Satellite-derived (shaded, from Bauman et al., 2003) and modelled (contours) effective radii (R_{eff}) in μm at 25 and 20 km from runs **A_Control20** (panels a and b) and **B_Control10** (panels c and d).

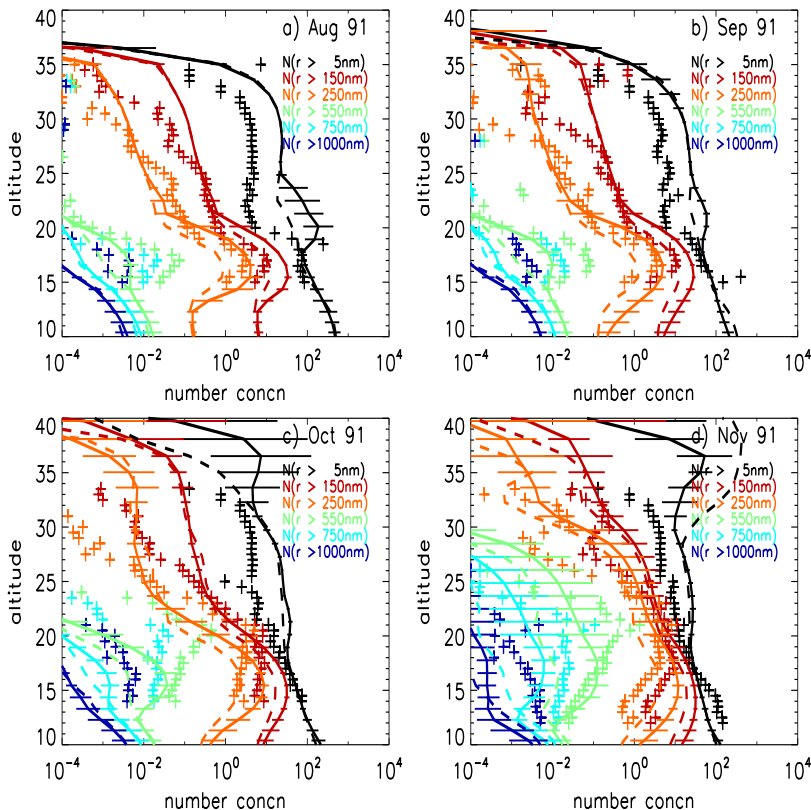


Fig. 9. August, September, October, November 1991 profiles of size-resolved number concentrations of particles (cm⁻³) with radii larger than 5, 150, 250, 550, 750 and 1000 nm from Laramie (41.3° N, 105.5° W) are shown with plus (+) symbol. Solid and dashed lines show aerosol profiles from the runs **A_Control20** and **B_Control10**, respectively highlighting the region where model predicts the perturbation in the aerosol profiles. Horizontal coloured lines represent standard deviations (1-σ) in number concentrations for a given month calculated from daily values for run **A_Control20**.

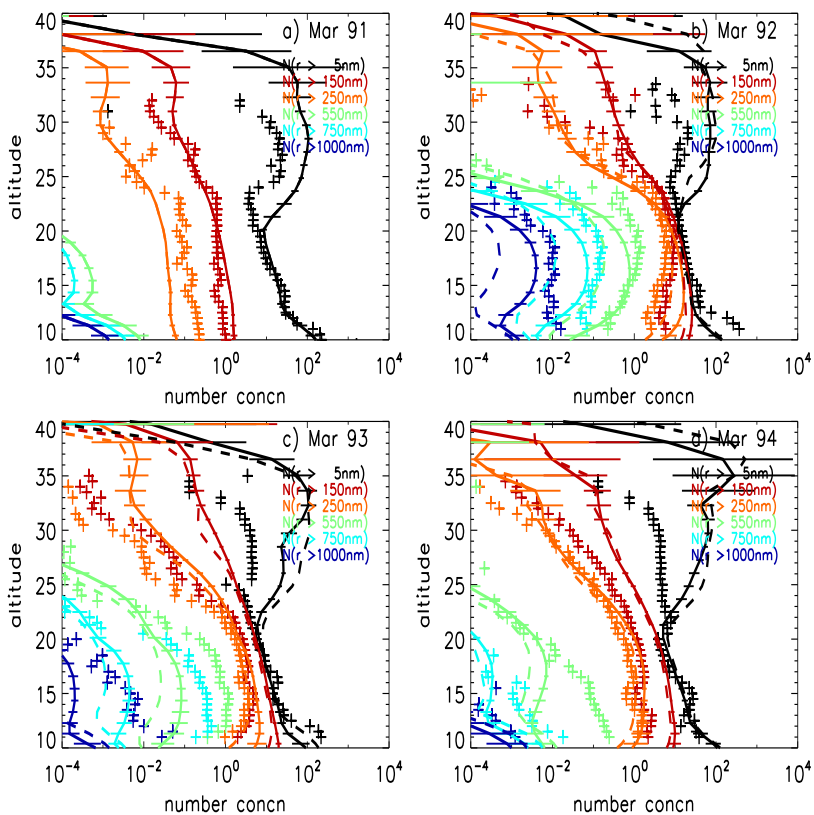
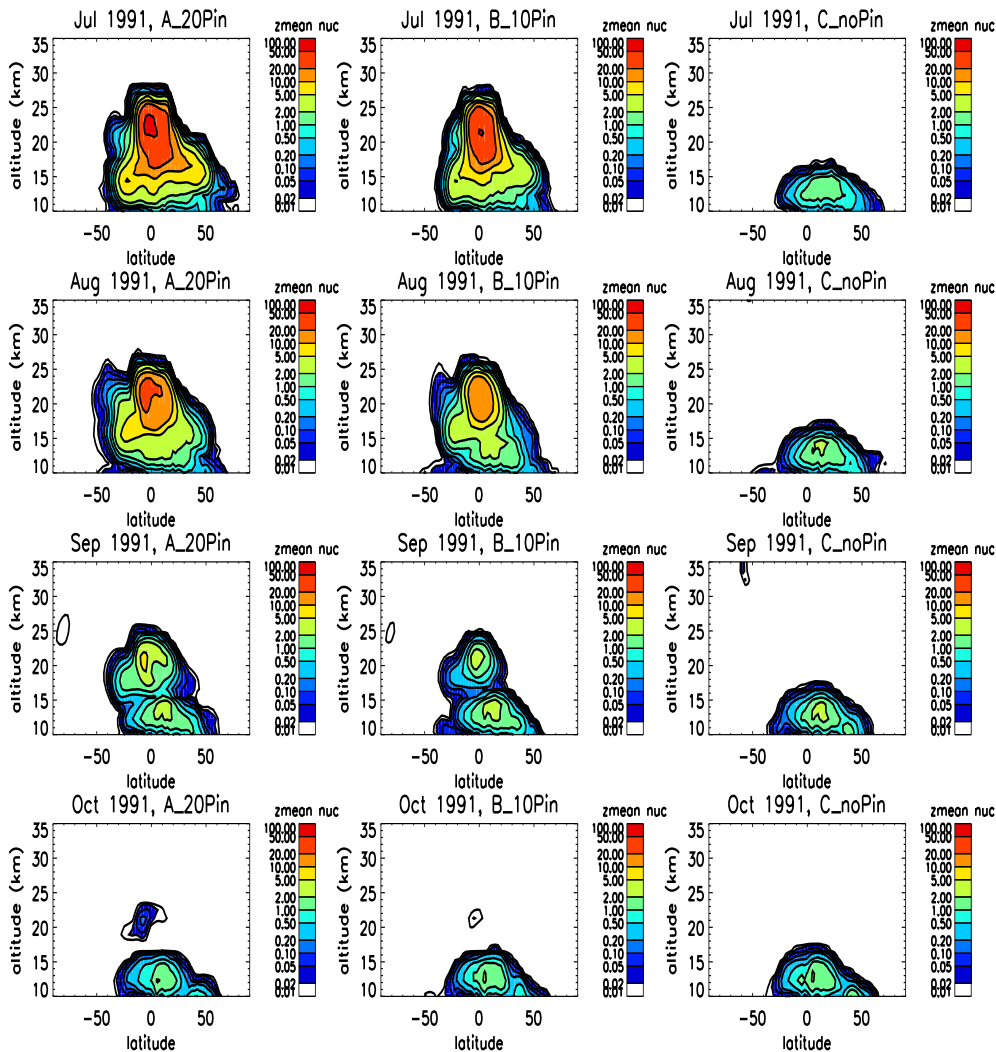


Fig. 10. Same as Fig. 9 but for March 1991, March 1992, March 1993 and March 1994.



60

Fig. 11. Modelled nucleation rates (cm^3s^{-1}) from runs **A_Control20** (left), **B_Control10** (middle), and **C_noPinatubo** (right) for (top to bottom) July, August, September and October 1991.

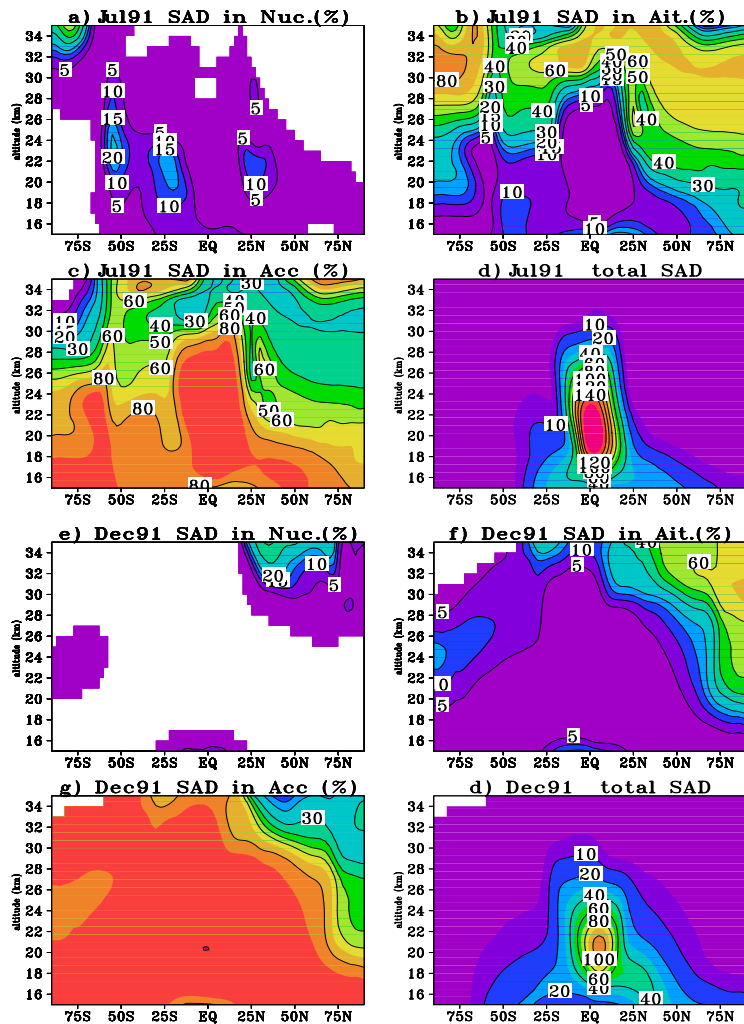


Fig. 12. Percentage zonal mean surface area densities in nucleation, Aitken and accumulation modes from run *A_Control20* for July 1991 (panels **a**, **b**, **c**) and December 1991 (panels **e**, **f**, **g**). Total SAD for July 1991 and December 1991 ($\mu^2\text{cm}^{-3}$) are shown in panel **(d)** and **(h)**,

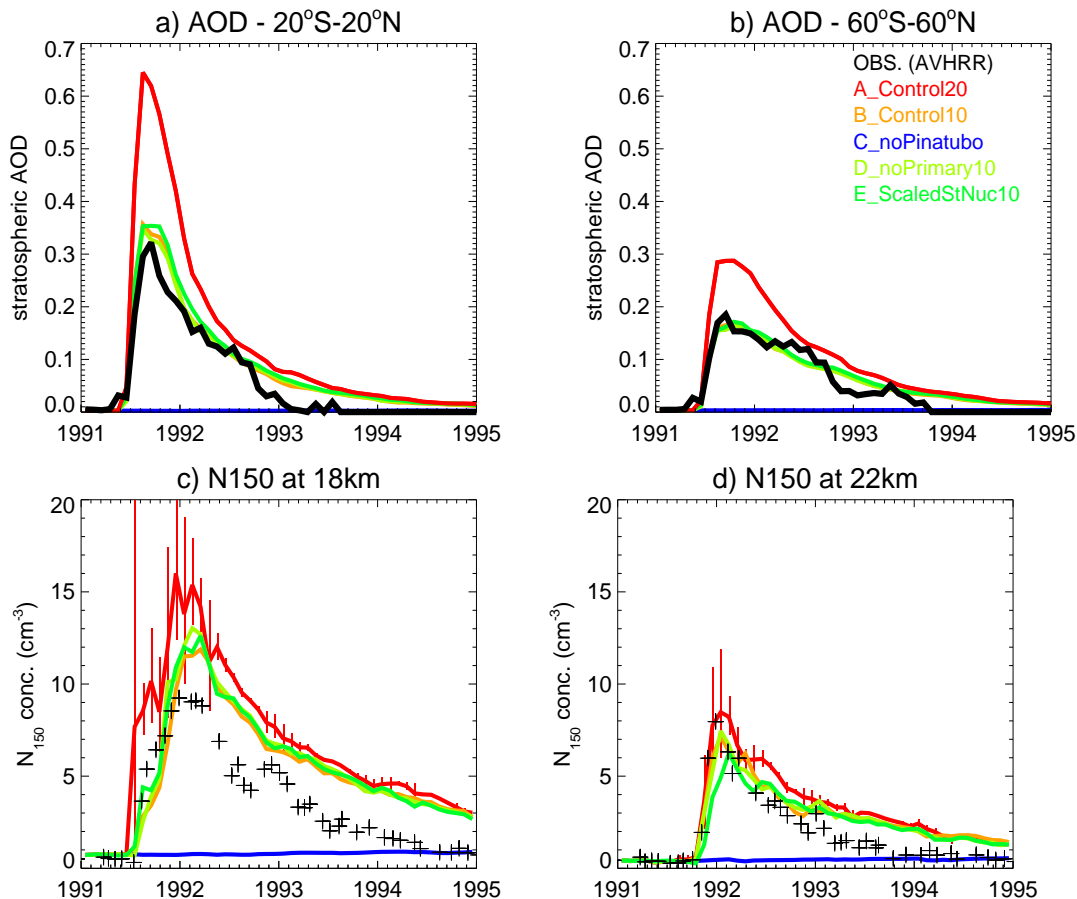


Fig. 13. Mean tropical (**a**, 20°S–20°N) and near-global (**b**, 60°S–60°N) AOD from AVHRR (550 nm) and various model simulations (525 nm). **c** and **d** show comparison between modelled and observed N_{150} timeseries from Laramie (shown with + sign), at 18 km and 22 km, respectively.